Optical Materials 80 (2018) 143–148

Contents lists available at ScienceDirect

Optical Materials

journal homepage: www.elsevier.com/locate/optmat

Enhancement in fluorescence quantum yield of MEH-PPV:BT blends for polymer light emitting diode applications

K.M. Nimith*, M.N. Satyanarayan, G. Umesh

Department of Physics, National Institute of Technology Karnataka, Surathkal, PO Srinivasnagar, Mangalore- 575025, Karnataka, India

ARTICLE INFO

Keywords:
Conjugated polymer
Fluorescence quantum yield
MEH-PPV
Benzothiadiazole
Polymer light emitting diodes
Electroluminescence

ABSTRACT

We have investigated the effect of blending electron deficient heterocycle Benzothiadiazole (BT) on the photophysical properties of conjugated polymer Poly [2-methoxy-5-(2-ethylhexyloxy)-1,4-phenylenevinylene] (MEH-PPV). Quantum yield (QY) value has been found to increase from 37% for pure MEH-PPV to 45% for an optimum MEH-PPV:BT blend ratio of 1:3. This can be attributed to the efficient energy transfer from the wide bandgap BT (host) to the small bandgap MEH-PPV (guest). The FTIR spectrum of MEH-PPV:BT blended thin film indicates suppression of aromatic C-H out-of-plane and in-plane bending, suggesting planarization of the conjugated polymer chains and, hence, leading to increase in the conjugation length. The increase in conjugation length is also evident from the red-shifted PL spectra of MEH-PPV:BT blended films. Single layer MEH-PPV:BT device shows lower turn-on voltage than single layer MEH-PPV alone device. Further, the effect of electrical conductivity of PEDOT:PSS on the current-voltage characteristics is investigated in the PLED devices with MEH-PPV:BT blend as the active layer. PEDOT:PSS with higher conductivity as HIL reduces the turn on voltage from 4.5 V to 3.9 V and enhances the current density and optical output in the device.

1. Introduction

Since the first report on organic/polymer light emitting diodes [1,2], there have been continuous efforts to improve the device efficiency and lifetime by employing novel device architectures and synthesizing new efficient organic materials [3–12]. Organic semiconductors (OSCs) are well suited for thin, light-weight, flexible and large area flat panel displays and solar cells. Organic Light Emitting Diodes (OLEDs), Solar Cells, Sensors and Lasers are some of the explored applications of OSCs [13–15]. Polymer light-emitting diodes (PLEDs) are of particular interest since they can be fabricated by low temperature solution processing and scalable technologies, such as inkjet printing, on large area flexible substrates [16,17]. Recent applications of PLEDs include flexible displays, solid-state lighting and short-range indoor optical communication [18–20].

Efficient charge injection, balanced charge transport, exciton formation and recombination within the active layer are the basic processes involved in the operation of a PLED [21]. However, it is well documented in the literature that the magnitude of hole transport in OSCs are a few orders greater than that of electron mobility, which is hindered by omnipresent electron traps at 3.6 eV [22]. The imbalance of charge carrier transport in the OSCs invariably results in poor device efficiency and performance. This problem has been partly addressed by the design and synthesis of new materials with balanced charge carrier transport and, also, by blending active layer material with electron transport material [23]. A multilayer device includes hole injection layer (HIL), hole transport layer (HTL), electron blocking layer (EBL) on one side of the electroluminescent (EL) layer and, hole blocking layer (HBL), electron transport layer (ETL), electron injection layer (EIL) between the EL layer and the cathode. Such devices show improved device performance [24]. However, a serious problem in such multilayer devices is the dissolution of pre-deposited polymer layer by the solution for the subsequent layer [25]. Hence, there is great interest in fabricating few-layer devices using blended polymer materials with good device efficiency [26].

Poly [2-methoxy-5-(2′-ethylhexyloxy)-1,4-phenylene vinylene] (MEH-PPV), a well-investigated electroluminescent conjugated polymer and Benzothiadiazole (BT), an electron deficient small molecule, have been widely used in the field of organic optoelectronics [27,28]. Recently, Bidgoli et al. have explored the possibility of blending these materials and applying it as a single electroluminescent layer in the polymer light emitting diodes [29,30]. The motivation behind this was to balance the charge carrier mobilities within the active layer and thereby avoiding the complexity of multilayer device structure. They could observe a reduction in the turn on voltage and an increase in the lifetime of these devices. However, an extensive study of the photo-

* Corresponding author.
E-mail address: nimithkm@gmail.com (K.M. Nimith).

https://doi.org/10.1016/j.optmat.2018.04.046
Received 10 November 2017; Received in revised form 22 April 2018; Accepted 23 April 2018

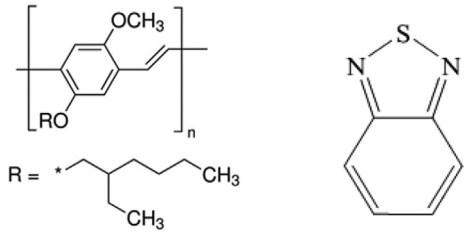

Fig. 1. Chemical structure of MEH-PPV and BT respectively (from Sigma-Aldrich website).

physical properties and different interaction mechanisms of these materials are still lacking in the literature. Here we report the enhancement in fluorescence quantum yield of MEH-PPV by the addition of BT. Fluorescence quantum yield (Φ_f), a measure of the efficiency of conversion of absorbed light into emitted light, is the key parameter for comparison of fluorophore efficiency. Relative fluorescence quantum yield can be easily measured using a UV–Vis spectrometer and a spectro-fluorometer.

2. Experimental details

MEH-PPV with a number averaged molecular weight (Mn) of 40000–70000 and with a polydispersity index (PDI) of around 6 and BT with a purity of 98% were purchased from Sigma Aldrich. Their chemical structures are shown in Fig. 1. Two varieties of PEDOT:PSS, one of conductivity (1 S/cm) grade (referred to as PEDOT:PSS1) and another with high-conductivity (> 200 S/cm) grade (PEDOT:PSS2) were also purchased from Sigma Aldrich. All these materials were used as received and without any further purification. Indium Tin Oxide (ITO) patterned glass substrates with sheet resistance of 15Ω/□ and thickness of 150 nm was sourced from Kintech, Taiwan, and used as the anode for the device fabrication. MEH-PPV and BT were separately dissolved in 1,2-dichorobenzene (DCB) to obtain solutions with a concentration of 1 mg/ml each. These two solutions were mixed together in different ratios to get appropriate weight percentages and subjected to the absorption and emission spectroscopy to investigate the effect of BT on the optical properties of MEH-PPV. Fluorescence quantum yields were calculated from the absorption and fluorescence spectra using a comparative method in which Fluorescein used as the standard.

UV–Vis absorption spectrum was recorded using Ocean Optics USB 4000 spectrophotometer with integration time of 30 ms. Fluorescence spectrum at room temperature was recorded using Horiba Jobin Yvon Fluoromax-4 spectrometer. Both the fluorescence reference standard and samples under the investigation were excited by light of wavelength 496 nm and the slit width of excitation and emission monochromators were kept 0.75 nm. FTIR spectrum of MEH-PPV and MEH-PPV:BT blend films were recorded by Perkin Elmer Frontier MIR spectrometer to investigate the structural changes and bond stretching or bending in MEH-PPV after blending with BT.

3. Results and discussions

3.1. Photo-physical studies of MEH-PPV and MEH-PPV:BT blends

Fig. 2 shows the normalized UV–Vis absorption curves for pure BT, pure MEH-PPV and for MEH-PPV:BT in a 1:3 blend in DCB solvent. The same curves were recorded for all other MEH-PPV:BT blend ratios (see the supporting information). The absorption spectrum shows characteristics absorption peak at 310 nm and 503 nm for solution of pure BT and MEH-PPV, respectively. The MEH-PPV:BT blend solution retains the absorption maxima at 310 nm, however, the absorption at 503 nm is much reduced. The absorption spectrum for 1:1 shows almost equal absorption for the constituent materials and is simply the linear combination of absorption spectrum of BT and MEH-PPV. As the weight

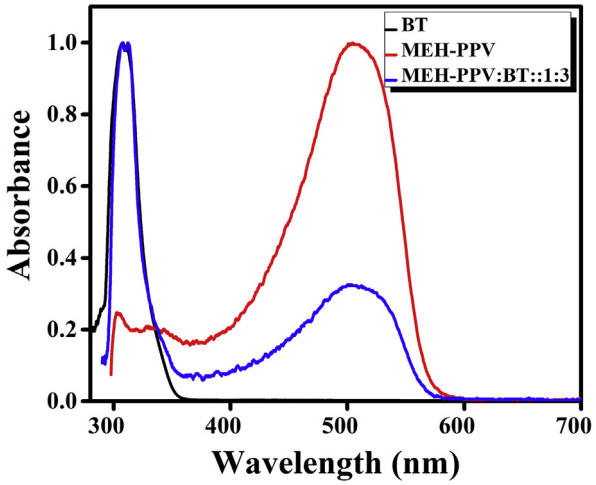

Fig. 2. Normalized UV–Vis absorption spectrum of MEH-PPV, BT and MEH-PPV:BT (1:3 ratio) solutions in DCB solvent.

percentage of MEH-PPV in the blend decreases, a similar reduction is seen in the absorbance. Optical bandgap of these materials was calculated by substituting the λ_{onset} value in the equation $E_g = \frac{1241.25}{\lambda_{onset}}$ eV, and found to be 3.55 eV and 2.18 eV for BT and MEH-PPV solutions, respectively. The calculated optical bandgap values are in good agreement with the values in the literature [31].

For very dilute solution (absorbance < 0.1) of BT, the excitation wavelength was 310 nm, corresponding to absorption maximum in UV–Vis, and the fluorescence emission (Fig. 3) was recorded from 325 nm to 600 nm. BT shows a narrow emission spectrum ranging from 350 nm to 450 nm with an emission maximum at 380 nm. MEH-PPV and MEH-PPV:BT solutions were excited with light at wavelength of 496 nm and the emission was recorded from 506 nm to 800 nm. Both the solutions show almost identical emission spectra without any shift in the peak wavelength. This suggests that blending has little effect on the shape of the PL spectrum and the optical band gap of MEH-PPV. Therefore, BT can be a good alternative for inducing the charge carrier balance in MEH-PPV without modifying the optical characteristics of MEH-PPV. Both MEH-PPV and MEH-PPV:BT blend solutions show a dominant peak at 569 nm and a shoulder at 610 nm, and their corresponding energy values are 2.18eV, 2.03eV respectively. Another shoulder peak at 668 nm (1.86eV) is barely visible. The energy difference between the three peaks are equal and it follows the usual vibronic progression [32]. A red shifted PL spectrum was obtained for both

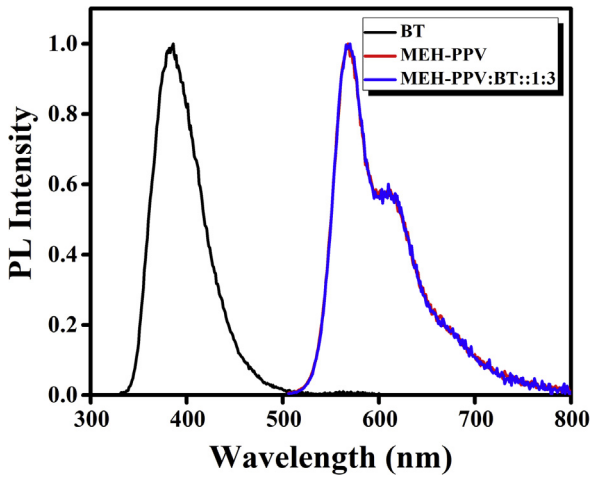

Fig. 3. Normalized fluorescence spectra of MEH-PPV, BT and MEH-PPV:BT (1:3 ratio) solutions in DCB solvent.

Table 1
Optical parameters obtained from the absorption and emission spectra.

Sample	Solvent	UV–Vis λ_{max} (nm)	PL λ_{max} (nm)	Stoke Shift λ_{PL}-λ_{UV} (nm)
MEH-PPV	DCB	503	570	67
BT	DCB	310	386	76
MEH-PPV:BT (1:3)	DCB	310, 503	568	65

Table 2
Fluorescence quantum yield values for different blend ratios of MEH-PPV with BT.

MEH-PPV:BT	1:0	1:1	1:2	1:3	1:4	1:5
QY (%)	37.48	40.79	42.96	45.54	38.67	38.26

MEH-PPV and MEH-PPV:BT blend (1:3 ratio) films compared to their solution state (see the supporting information).

The optical parameters obtained from the absorption and emission spectra are presented in Table 1.

Fluorescence quantum yield (Φ_f) is simply the ratio of number of photons emitted to the number of photons absorbed. Here we have adopted the commonly used comparative fluorescence quantum yield measurement technique taking fluorescein, dissolved in 0.1 M NaOH solution, as the reference standard whose QY value, taken from the literature is 0.95. Fluorescence quantum yield (Φ_f) is given by Refs. [33–35].

$$\Phi_{f,x} = \Phi_{f,st}\frac{F_x}{F_{st}}\frac{f_{st}}{f_x}\frac{n_x^2(\lambda_{em})}{n_{st}^2(\lambda_{em})} \quad (1)$$

Here F is the integral photon flux, f is the absorption factor, n is the refractive index (at the excitation wavelength) of the solvent and Φ_f is the quantum yield. The index x denotes the sample and the index st denotes the standard solution. F_x and F_{st} values were obtained by integrating the PL spectra over wavelength. The absorption factor is given by $f = 1 - 10^{-A(\lambda_{ex})}$, where $A(\lambda_{ex})$ is the absorbance at the excitation wavelength. Absorption factor can be considered as the absorbance value at the excitation wavelength for very dilute solution. All the solutions were taken in a quartz cuvette having a path length of 10 mm and were subjected to both absorption and fluorescence measurements. Here all the solution concentrations were restricted to get absorbance values less than 0.1 to ensure that self-absorption is negligible.

Here we substituted 1.335 and 1.551 for the refractive index value (at 589 nm) of the 0.1 M NaOH and DCB solvents, respectively. The slope values were extracted from the absorbance versus integrated fluorescence intensity graph (Fig. 4) and substituted in equation (1). The quantum yield values obtained for different blend ratios of MEH-PPV:BT are tabulated Table 2.

From the calculated QY values it is clear that the fluorescence quantum yield increases initially with increasing proportion of BT in the blend and attains a maximum QY value of 45% for MEH-PPV:BT blend ratio of 1:3. Further blending of BT into MEH-PPV resulted in reducing the QY value to 38% for blend ratio of 1:4 and more. Efficient energy transfer from a wide bandgap host to a small bandgap guest happens only when the emission spectrum of the host overlaps considerably with the absorption spectrum of the guest [6]. Since the emission spectrum of BT overlaps to some extent with the absorption spectrum of MEH-PPV, shown in Fig. 5, the energy transfer from the host BT to the guest MEH-PPV must be considered. The extent of overlap between the emission spectrum of BT and absorption spectrum of MEH-PPV was further improved when the blended liquid was cast into a solid film form (see the supporting information). This energy transfer can, in turn, result in the enhancement of fluorescence QY for MEH-PPV:BT blend.

Since MEH-PPV:BT:1:3 blend ratio resulted in maximum fluorescence QY, further characterizations and device fabrication were done using MEH-PPV:BT blend solution with 1:3 blend ratio only.

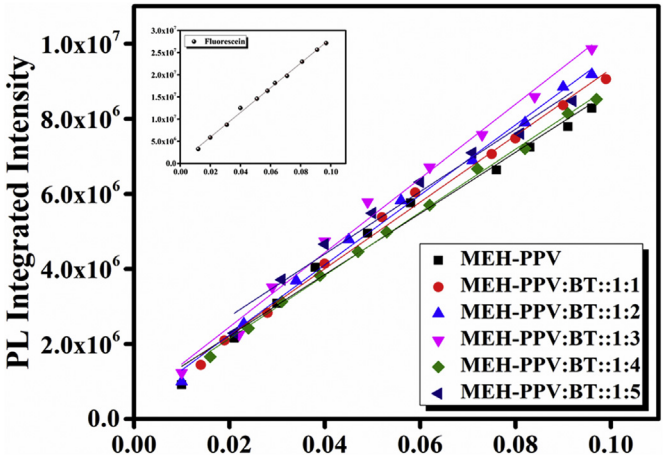

Fig. 4. Absorbance versus integrated fluorescence intensity graph for different blend ratios of MEH-PPV and BT. The same graph for fluorescein is shown in the inset. The absorbance values were recorded at a wavelength of 496 nm for both the sample and standard solutions.

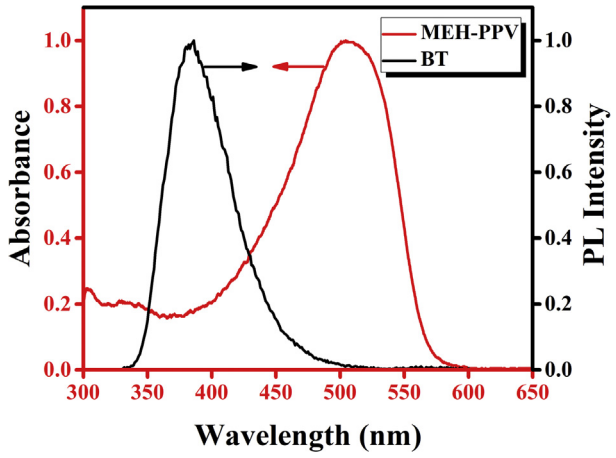

Fig. 5. Normalized absorption spectrum of MEH-PPV and PL emission spectrum of BT.

Infrared spectra of MEH-PPV and MEH-PPV:BT films were recorded by ATR method, from an upper limit 4000 cm^{-1} down to 650 cm^{-1}, to investigate whether there are any structural changes and bond stretching or bending in MEH-PPV after blending with BT. FTIR spectrum of the glass substrate was recorded as the reference. FTIR spectrum of MEH-PPV:BT blend film shown in Fig. 6 is similar to that of MEH-PPV except for the absence of vibrational frequencies at 727, 853, 1080, 1117, 1152, 2212, 3106 cm^{-1}. The absence of certain group frequencies implies that the blending results in reduced methylene-$(CH_2)_n$ – rocking and absence of aromatic C-H out-of-plane and in-plane bend [36]. The absence of aromatic C-H out-of-plane and in-plane bend in the MEH-PPV:BT blend can lead to planarization of the conjugated polymer chains and, thus, an increased conjugation length. The increase in conjugation length is further confirmed from the red-shifted PL spectra for MEH-PPV:BT blended films compared to MEH-PPV film [32,37]. In the PL spectra, full width at half maxima is 31 nm for MEH-PPV film and it reduces to 25 nm for MEH-PPV:BT blended films. The narrowing of the emission spectrum can be due to the dilution effects that decrease the conformational disorder in the blended films [32,38]. The conformational modification and the increased conjugation length can lead to an enhancement in the fluorescence quantum yield of MEH-PPV:BT thin films [38,39].

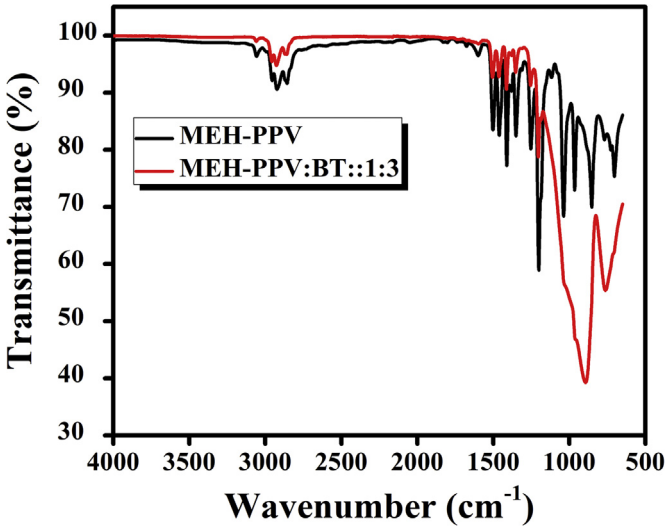

Fig. 6. FTIR spectra of MEH-PPV and MEH-PPV:BT thin films on glass substrate.

3.2. Polymer light emitting diodes (PLEDs) using MEH-PPV:BT blend

For the device fabrication, MEH-PPV and BT were separately dissolved in DCB at 5 mg/ml and blended together in the weight ratio 1:3. Single and multi-layer PLEDs were fabricated using this MEH-PPV:BT blend for the active layer since the blend ratio of 1:3 resulted in maximum fluorescence quantum yield. The device structure and the energy level diagram of the materials used in the devices are shown in Fig. 7. The blended solution was spin cast at a speed of 2000 rpm for 30 s. The amorphous nature of the MEH-PPV and MEH-PPV:BT blend films were confirmed by X-ray diffraction (XRD) and is presented in the supporting information. Active layer thickness of 100 nm was obtained by step height measurement of MEH-PPV:BT film using Atomic Force Microscope (AFM), in tapping mode (Bruker- Dimension Icon). Several multilayer devices were fabricated using PEDOT:PSS, of two different conductivities, as HIL and its effect on the device performance was investigated. The two PEDOT:PSS solutions were spin cast at 2000 rpm for 30 s yielding films of thickness 20 nm for PEDOT:PSS1 and 60 nm for PEDOT:PSS2, respectively. Aluminum film of thickness 120 nm was deposited as the cathode by thermal evaporation at a vacuum level of 5×10^{-6} mbar.

The current density-voltage characteristics of the devices, were recorded under ambient conditions just after the fabrication. Fig. 8 indicates that the high conductive PEDOT:PSS film works as a good hole injection layer and drastically reduces the turn on voltage, thereby increasing the current density in the devices. The turn on voltage for devices with high conductivity PEDOT:PSS2 is 3.9 V where as that of devices with lower conductivity PEDOT:PSS1 is 4.5 V. Clearly, the high conductivity PEDOT:PSS film plays the role of a good HIL. The J-V characteristics of MEH-PPV single layer device shows a higher turn on voltage (12 V) than the MEH-PPV:BT (1:3) single layer device (9 V).

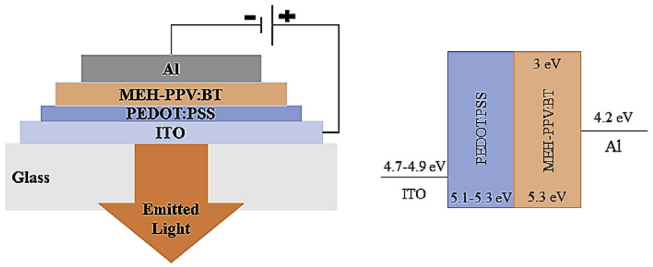

Fig. 7. Device structure and energy level diagram of multilayer PLEDs with MEH-PPV:BT as active layer.

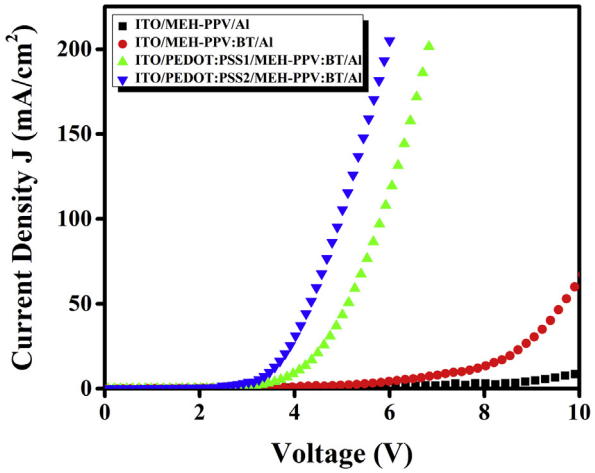

Fig. 8. Current density-voltage (J–V) characteristics of MEH-PPV:BT (1:3) blend devices with and without PEDOT:PSS film of different conductivities as HIL. J-V characteristics of MEH-PPV alone device is also shown for comparison.

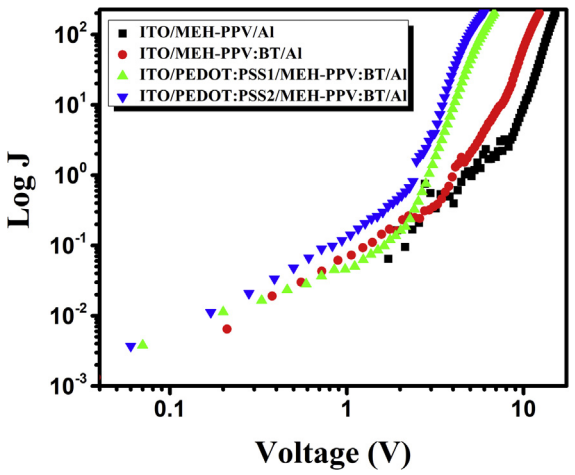

Fig. 9. Logarithmic plot of current density-voltage (J–V) characteristics of MEH-PPV:BT blend (1:3 ratio) devices with and without PEDOT:PSS as HIL.

The logarithmic (J-V) plot (Fig. 9) for single layer MEH-PPV:BT blend devices shows three distinct linear regions conforming to a power law behaviour ($J \alpha V^{k+1}$) [29]. At low voltages current injection mechanism is dominated by ohmic injection having a slope value of 0.90. At intermediate voltages, the conduction mechanism changes from ohmic to space charge limited (SCLC) type, with a slope value of 1.50. SCLC is exhibited by low-mobility semiconductor materials when the injected charge density is far greater than the intrinsic free carrier density. As the voltage increases further, the k value also increases to 4.98, signifying the domination of trap charge limited conduction (TCLC). Multilayer devices, having PEDOT:PSS and MEH-PPV:BT layers, also exhibit a similar behaviour with three distinct linear regions. Slope values of 0.94, 1.96 and 6.08 were obtained for devices with PEDOT:PSS1 and 1.05, 1.6 and 6.13 for devices with higher conductivity PEDOT:PSS2 layer as HIL.

In order to estimate the surface roughness of the PEDOT:PSS films, the morphology of the films have been studied using AFM. The AFM images (Fig. 10) of PEDOT:PSS films, yield a surface roughness rms value (Rq) of 2.85 nm for PEDOT:PSS2 and 3.48 nm for PEDOT:PSS1. Although the AFM images of PEDOT:PSS2 film looks highly granular, NanoScope software analysis shows lower surface roughness for PEDOT:PSS2. Therefore the high conductive PEDOT:PSS2 can form a better interface with the MEH-PPV:BT emissive layer and, hence, enhances the charge injection into MEH-PPV:BT layer.

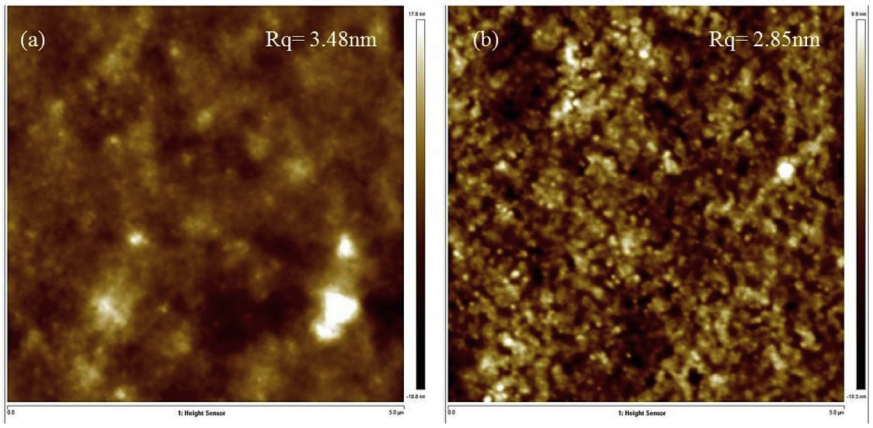

Fig. 10. Surface roughness of (a) PEDOT:PSS1 (b) PEDOT:PSS2 thin films on glass substrates using AFM at a scan area of 5 μm × 5 μm.

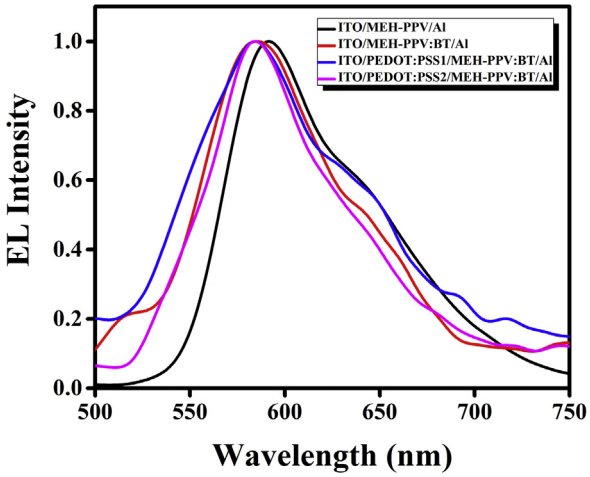

Fig. 11. Normalized electroluminescence (EL) spectra of the devices with MEH-PPV alone and MEH-PPV:BT:1:3 blend as active layers. EL recorded at a bias voltage corresponding to the current density of ~100 mA/cm^2 for all the devices (5 V, 6 V, 11 V and 14 V, respectively for ITO/MEH-PPV/Al, ITO/MEH-PPV:BT/Al, ITO/PEDOT:PSS1/MEH-PPV:BT/Al, ITO/PEDOT:PSS2/MEH-PPV:BT/Al devices).

Fig. 11 shows the electroluminescence (EL) spectrum of the devices with MEH-PPV alone and MEH-PPV:BT blend, as active layer. The EL spectra were recorded over a wavelength range 300–800 nm using a spectrometer (Flame, Ocean Optics). The EL spectrum was trimmed between 500 and 750 nm to avoid the noise present in it. All the devices exhibit a broad EL ranging from a wavelength of 525 nm–725 nm. Emission maxima occurs close to 591 nm wavelength for MEH-PPV based devices and at 586 nm for MEH-PPV:BT based devices. The small blue shift in the emission maxima of MEH-PPV:BT devices can be due to the interaction between MEH-PPV and BT. It is well documented that the PL spectrum of the fluorescent molecules shows a red shift in the solid state compared to the respective solution state. The PL spectrum resembles the EL spectrum for these materials. The PL spectrum of BT solution shows the emission maxima at 386 nm and is expected to exhibit a red shifted EL emission in film form. Hence, the strong EL emission at 586 nm from the MEH-PPV:BT device may be ascribed to MEH-PPV only [40].

The optical output measurement shows that same current density (~100 mA/cm^2) resulted in higher number of photons (integration from 400 nm to 700 nm) for single layer MEH-PPV:BT blended device (1.69×10^{10}) than the single layer MEH-PPV alone device (8.23×10^{9}). From the optical and electrical characterizations, it is clear that blending MEH-PPV and BT together and applying it as an active layer resulted in a lower turn-on voltage and better device efficiency than MEH-PPV alone device. Further, multilayer device with PEDOT:PSS as HIL improves the optical output due to better hole injection. Device with high conductivity PEDOT:PSS2 as HIL shows improved optical output and large number of photons (2.61×10^{10}) than the device with lower conductive PEDOT:PSS1 (2.49×10^{10}).

4. Summary and conclusions

Fluorescence quantum yield (Φ) measurement reveals that the addition of BT into MEH-PPV resulted in an enhancement in the fluorescence efficiency. A maximum quantum yield of 45% obtained for an optimum blend ratio of 1:3 for MEH-PPV:BT. This can be attributed to the efficient energy transfer from the wide bandgap host to the small bandgap guest. FTIR spectra revealed the suppression of aromatic C-H out-of-plane and in-plane bending in the MEH-PPV:BT blend. This leads to the planarization of the conjugated polymer chains and increased conjugation length. Single layer MEH-PPV:BT device shows lower turn on voltage and higher optical output than single layer MEH-PPV alone device. Use of high conductivity PEDOT:PSS film as HIL enhances the charge injection into the active polymer and reduces the turn on voltage of the device. AFM image shows a smoother surface for the high conductivity PEDOT:PSS films and therefore forms a better interface between HIL and active polymer layer resulting in enhanced charge injection. Blending of MEH-PPV and BT does not affect the photo-physical properties of MEH-PPV and the EL originates only from MEH-PPV. Therefore, BT is seen to be a good candidate to induce balanced charge carrier transport and obtain emission enhancement in MEH-PPV based PLEDs, with less device complexity.

Acknowledgements

A portion of this research was performed using facilities at CeNSE, funded by Ministry of Electronics and Information technology (MeitY), Govt. of India, and located at the Indian Institute of Science, Bengaluru. KMN is grateful to N.I.T.K., Surathkal, for granting him a research fellowship.

Appendix A. Supplementary data

Supplementary data related to this article can be found at http://dx.doi.org/10.1016/j.optmat.2018.04.046.

References

[1] C.W. Tang, S.A. Vanslyke, Organic electroluminescent diodes, Appl. Phys. Lett. 51 (1987) 913–915.
[2] J.H. Burroughes, et al., Light-emitting diodes based on conjugated polymers, Nature

347 (1990) 539–541.
[3] D.L. Sivco, A.Y. Cho, G.J. Zydzik, Highly Efficient Lig Ht-Emitting Diodes with Microcavities vol. 265, (1994).
[4] V. Bulovic, G. Gu, P.E. Burrows, S.R. Forrest, M.E. Thompson, Transparent light-emitting devices, Nature 380 (1996) 29.
[5] S.R. Forrest, et al., The stacked OLED (SOLED): a new type of organic device for achieving high-resolution full-color displays, Synth. Met. 91 (1997) 9–13.
[6] M.A. Baldo, et al., Highly efficient phosphorescent emission from organic electroluminescent devices, Nature 395 (1998) 151–154.
[7] S. Reineke, et al., White organic light-emitting diodes with fluorescent tube efficiency, Nature 459 (2009) 234–238.
[8] A. Endo, et al., Thermally activated delayed fluorescence from Sn4 + -Porphyrin complexes and their application to organic light emitting diodes - a novel mechanism for electroluminescence, Adv. Mater. 21 (2009) 4802–4806.
[9] S. Reineke, M. Thomschke, B. Lussem, K. Leo, White organic light-emitting diodes: status and perspective, Rev. Mod. Phys. 85 (2013) 1245–1293.
[10] Q.D. Ou, et al., Extremely efficient white organic light-emitting diodes for general lighting, Adv. Funct. Mater. 24 (2014) 7249–7256.
[11] J.K. Kim, et al., Origin of white electroluminescence in graphene quantum dots embedded host/guest polymer light emitting diodes, Sci. Rep. 5 (2015) 1–11.
[12] M.Y. Wong, Recent advances in polymer organic light-emitting diodes (PLED) using non-conjugated polymers as the emitting layer and contrasting them with conjugated counterparts, J. Electron. Mater. (2017), http://dx.doi.org/10.1007/s11664-017-5702-7.
[13] A. Dickinson, T, J. White, J.S. Kauer, Lasing from conjugated polymer Microcavities.pdf, Nature 382 (1996) 695–697.
[14] Hu, W. Organic Electronics II Organic Photovoltaics Physics of Organic Semiconductors Physical and Chemical Aspects of Organic Electronics.
[15] X. Dai, et al., Solution-processed, high-performance light-emitting diodes based on quantum dots, Nature 515 (2014) 96–99.
[16] R.H. Friend, et al., Electroluminescence in conjugated polymers, Natalia 397 (1999) 121–128 www.nature.com.
[17] H. Zheng, et al., All-solution processed polymer light-emitting diode displays, Nat. Commun. 4 (2013) 1971.
[18] G. Gustafsson, et al., Flexible light-emitting-diodes made from soluble conducting polymers, Nature 357 (1992) 477–479.
[19] M.S. White, et al., Ultrathin, highly flexible and stretchable PLEDs, Nat. Photon. 7 (2013) 811–816.
[20] P.A. Haigh, et al., Visible light communications: real time 10 Mb/s link with a low bandwidth polymer light-emitting diode, Optic Express 22 (2014) 2830.
[21] X.-Y. Deng, Light-emitting devices with conjugated polymers, Int. J. Mol. Sci. 12 (2011) 1575–1594.
[22] H.T. Nicolai, et al., Unification of trap-limited electron transport in semiconducting polymers, Nat. Mater. 11 (2012) 882–887.
[23] P. Cea, et al., A blended layer MEH-PPV electroluminiscent device incorporating a new electron transport material, Mater. Sci. Eng. C 22 (2002) 87–89.
[24] N. Prasad, et al., Improving the performance of MEH-PPV based light emitting diode by incorporation of graphene nanosheets, J. Lumin. 159 (2015) 166–170.
[25] C. Newby, J.K. Lee, C.K. Ober, The solvent problem: redissolution of macromolecules in solution-processed organic electronics, Macromol. Res. 21 (2013) 248–256.
[26] D. Abbaszadeh, et al., Elimination of charge Carrier trapping in diluted semiconductors, Nat. Mater. 15 (2016) 628–633.
[27] P. Herguth, X. Jiang, M.S. Liu, A.K. Jen, Highly Efficient Fluorene- and Benzothiadiazole-based Conjugated Copolymers for Polymer Light-emitting Diodes, (2002), pp. 6094–6100.
[28] Y. Tao, et al., Synthesis and characterization of efficient luminescent materials based on 2, 1, 3-benzothiadiazole with carbazole moieties, Synth. Met. 161 (2011) 718–723.
[29] M.M. Bidgoli, M. Mohsennia, F.A. Boroumand, A.M. Nia, Optoelectronic characteristics of MEH-PPV + BT blend thin films in polymer light emitting diodes, Semicond. Sci. Technol. 30 (2015) 065016.
[30] M. Mohsennia, M.M. Bidgoli, F.A. Boroumand, A.M. Nia, Electrically conductive polyaniline as hole-injection layer for MEH-PPV: BT based polymer light emitting diodes, Mater. Sci. Eng. B 197 (2015) 25–30.
[31] E. Xu, et al., The synthesis and properties of novel pi -conjugated 2,1,3-benzothiadiazole oligomers, Dyes Pigments 80 (2009) 194–198.
[32] V.S. Reddy, A. Dhar, Ã. Optical and charge Carrier transport properties of polymer light emitting diodes based on MEH-PPV, Phys. B Phys. Condens. Matter 405 (2010) 1596–1602.
[33] C. Würth, M. Grabolle, J. Pauli, M. Spieles, U. Resch-genger, Relative and absolute determination of fluorescence quantum yields of transparent samples, Nat. Protoc. 8 (2013) 1535–1550.
[34] Christian Würth, Markus Grabolle, Jutta pauli, Monika Spieles, U. R.-G. Comparison of methods and achievable uncertainties for relative and absolute measurements of photoluminescence quantum yields, Anal. Chem. 83 (2011) 3431–3439.
[35] A.M. Brouwer, Standards for photoluminescence quantum yield measurements in solution (IUPAC Technical Report), Pure Appl. Chem. 83 (2011) 2213–2228.
[36] J. Coates, Interpretation of infrared spectra, a practical approach interpretation of infrared spectra, a practical approach, Encycl. Anal. Chem (2000) 10815–10837, http://dx.doi.org/10.1002/9780470027318.
[37] S. Giri, C.H. Moore, J.T. Mcleskey, P. Jena, Origin of red shift in the photoabsorption peak in MEH − PPV polymer, J. Phys. Chem. C 118 (2014) 13444–13450.
[38] A. Marletta, V.C. Gonçalves, D.T. Balogh, Effect of temperature on emission of MEH-PPV/PS solid-state solution, J. Lumin. 116 (2006) 87–93.
[39] I. Botiz, et al., Enhancing the photoluminescence emission of conjugated MEH-PPV by light processing, ACS Appl. Mater. Interfaces 6 (2014) 4974–4979.
[40] M. Berggren, et al., Light-emitting-diodes with variable colors from polymer blends, Nature 372 (1994) 444–446.

Synthetic Metals 250 (2019) 99–103

Contents lists available at ScienceDirect

Synthetic Metals

journal homepage: www.elsevier.com/locate/synmet

Capacitance and impedance spectroscopy studies of polymer light emitting diodes based on MEH-PPV:BT blends

K.M. Nimith*, N.S. Sterin, P.P. Das, G. Umesh, M.N. Satyanarayan

Department of Physics, National Institute of Technology Karnataka (NITK), Surathkal, PO Srinivasnagar, Mangalore, 575025, Karnataka, India

ARTICLE INFO

Keywords:
Polymer light emitting diodes
PLED
Conjugated polymer
Impedance Spectroscopy
IS
Nyquist plot
Capacitance
Conductance
Charge transport
Charge carrier mobility
Poly[2-methoxy-5-(2-ethylhexyloxy)-1,4-phenylenevinylene]
MEH-PPV
Benzothiadiazole
BT
Negative capacitance
NC

ABSTRACT

Light emitting polymer poly [2-methoxy-5-(2-ethylhexyloxy)-1,4-phenylenevinylene] (MEH-PPV) is blended with a wide bandgap electron transport material benzothiadiazole (BT) and its effect on the electronic properties has been studied by capacitance and impedance spectroscopy (IS) in PLEDs. The impedance data is fitted using equivalent circuit models and the minimum parallel resistance (Rp) at zero bias have been obtained for 1:3 ratio of MEH-PPV:BT blended devices. The negative capacitance (NC) shows the occurrence of the trap-assisted non-radiative recombination mechanism at low frequencies in the unblended MEH-PPV PLEDs. Further, this behavior is seen to be reduced in PLEDs with MEH-PPV:BT blends. This clearly suggests that the blending of MEH-PPV and BT at different weight ratios results in the suppression of trap-assisted recombination. This can be attributed to the elimination of trap states due to the dilution of semiconductor material on account of the addition of wide bandgap host material. Moreover, the blended devices have shown a significant improvement in the conductivity at small bias voltages.

1. Introduction

Organic semiconductors (OS) based solid-state lighting and flexible, light-weight, large-area display devices are now globally entering consumer market [1–6]. At the heart of such devices are organic semiconductors, which, compared to their inorganic counterparts have attracted attention due to the low-cost solution processability [7] and vacuum evaporation techniques [8] that can be employed for such materials. Efficient injection and balanced transport of charge carriers, exciton formation and recombination leading to radiative emission are the basic processes involved in the operation of an OLED/PLED [9]. Charge transport is an important parameter that influences the device efficiency. Unbalanced charge carrier transport can lead to poor device performance. Efficient injection of charge carriers can be realized by careful selection of electrode materials and addition of charge carrier injection and transport layers. Hence, it is now well understood in the research community that charge transport studies are of fundamental importance for designing and fabricating devices with improved efficiency. In the context of organic semiconductors, the commonly used techniques to determine the charge carrier mobility are: Time of Flight (TOF), Space-Charge-Limited Current (SCLC), Carrier Extraction by Linearly Increasing Voltage (CELIV), Double Injection (DoI) Transient Technique, Field Effect Transistor (FET), Capacitance-Voltage (C-V) analysis and Impedance Spectroscopy (IS). Each method has its own merits and demerits and excellent reviews detailing these techniques are available in literature [10–14].

The focus of this paper is on capacitance and impedance based spectroscopic techniques since it enables the simultaneous extraction of many physical quantities through fully automated measurements. C-V and IS are powerful and non-invasive techniques to understand the charge injection and transport in OSs [15], nature of metal-organic and organic-organic interfaces, the stability and degradation of OLED [16], and to determine the localized defect-state distribution [17]. IS uses a small alternating current (ac) perturbation superimposed on a dc voltage and probes the corresponding response from the device. The electron and hole mobility are simultaneously obtained for a single PLED using admittance spectroscopy [18]. Negative differential capacitance (NC) occurring at low frequencies is often seen in bipolar OLEDs

* Corresponding author.
E-mail address: nimithkm@gmail.com (K.M. Nimith).

https://doi.org/10.1016/j.synthmet.2019.03.009
Received 20 December 2018; Received in revised form 15 February 2019; Accepted 9 March 2019

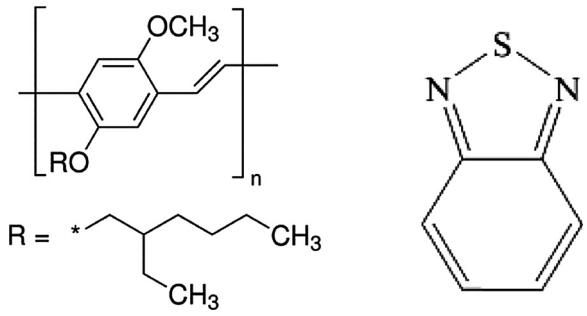

Fig. 1. Chemical structures of MEH-PPV and BT respectively (from Sigma-Aldrich website).

and has recently been attributed to the trap-assisted non-radiative recombination [19]. NC effect can be exploited to quantitatively determine the number of traps in OSs in a non-destructive fashion.

Bidgoli et al. have explored the possibility of blending MEH-PPV and BT together and applying it as a single electroluminescent layer in the polymer light emitting diodes [20,21]. Recently, Nimith et al. have reported an enhancement in the fluorescence quantum yield (QY) of MEH-PPV:BT blends [22]. Since the above material combination has shown to improve the optoelectronic properties of the device, understanding the basic mechanism involved in the charge transport is of fundamental importance for designing and fabricating devices with improved performance. Here the authors have explored the effect of blending on the electronic properties using capacitance and impedance based spectroscopic techniques in PLEDs.

2. Experimental techniques

MEH-PPV and BT were purchased from Sigma Aldrich and used as received. The chemical structures of these materials are shown in Fig. 1. Both the materials were dissolved in 1,2-dichlorobenzene (DCB) at 10 mg/ml and blended together. Since MEH-PPV:BT blend ratio of 1:3 yielded maximum fluorescence quantum yield (QY) in our previous studies, use of 1:3 blend ratio was explored here as the active layer for PLEDs. The pre-patterned ITO coated glass substrates with a sheet resistance of 15 Ω/□ were pre-cleaned following a standard procedure of ultrasonication in acetone and IPA for 30 min each, followed by UV-ozone treatment for 25 min. The blend solution was then spin-coated on the cleaned ITO coated glass substrates. The top Al electrode (120 nm) was deposited through a shadow mask in a thermal evaporator at a base pressure of 7×10^{-6} mbar. The device active area was 4 mm^2.

The frequency dependent capacitance (C-f), capacitance-voltage (C–V) and impedance measurements were carried out at room temperature using an impedance analyzer (Keysight E4990A) and a custom-made probe station. An ac voltage of 100 mV was superimposed on the dc bias and the measurements were carried out over a frequency range of 20 Hz- 2 MHz. The current-voltage (I–V) characteristics were recorded using a computer-controlled SMU (Keithley 2614B).

3. Results and discussions

Single layer PLEDs with three different device structures have been fabricated: ITO/MEH-PPV/Al, ITO/MEH-PPV:BT (1:1)/Al, ITO/MEH-PPV:BT (1:3)/Al and are designated as D_0, D_1, and D_3, respectively. Single layer unblended MEH-PPV PLEDs (D_0) were fabricated for comparison purposes. The current density-voltage (J-V) characteristics of the three devices are shown in Fig. 2. At reverse bias, the current density is almost negligible and constant. The current density increases drastically above the turn-on voltage. It is evident from the graph that the turn-on voltage is lower for the devices with MEH-PPV:BT blend as the active layer compared to unblended MEH:PPV devices. This is in accordance with our earlier work [22].

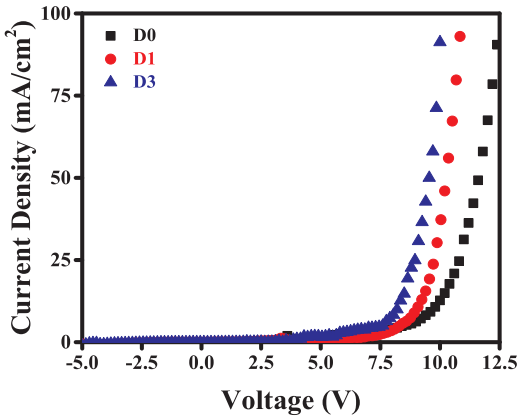

Fig. 2. Current density-voltage (J-V) characteristics of all the three devices.

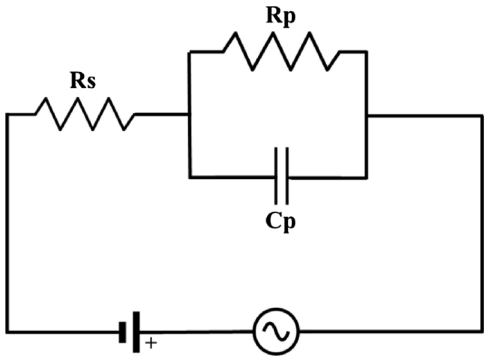

Fig. 3. Equivalent circuit model of a single layer PLED during impedance spectroscopy.

As for the electrical model of the fabricated devices, a single layer PLED can be modeled parallel combination of resistor (R_p) and capacitor (C_p) connected in series with a resistor R_s as shown in Fig. 3. The capacitor C_p represents the capacitive component (frequency independent) of the device and the parallel resistor R_p accounts for leakage current through the device. The series resistor R_s represents the contact resistance which originates from the ITO-OS, OS-Al interfaces and lead wires [23]. The complex impedance of this circuit is expressed in terms of the real and imaginary part as [24]:

$$Z = R_s + \frac{R_p - j\omega {R_p}^2 C_p}{1 + \omega^2 {R_p}^2 {C_p}^2} = Z' - jZ''$$

where $Z' = R_s + \frac{R_p}{1+\omega^2 {R_p}^2 {C_p}^2}$ and $Z'' = \frac{\omega {R_p}^2 C_p}{1+\omega^2 {R_p}^2 {C_p}^2}$

Fig. 4 shows the frequency-dependent real part of the impedance in device D_3 at different bias voltages. The same curves for the device D_1 have been shown in the supporting information. For a particular bias voltage, the impedance value is almost constant at low frequencies, decreases at intermediate frequencies (10^2 – 10^5 Hz) and finally attains a constant value at higher frequencies (> 10^5 Hz). As is also evident from the figure, the impedance value at low frequencies progressively decreases with increase in bias voltage. Interestingly, the falling edge of impedance curve shifts to higher frequencies as the bias voltage increases. At frequencies greater than 10^5 Hz impedance curves at all bias voltages converge.

The frequency-dependent imaginary part of the impedance in device D_3 is shown in Fig. 5. For a particular voltage, it is observed from the figure that Z" increases at lower frequencies and reaches a maximum value, and then finally decreases at higher frequencies. With increase in bias voltage, the peak of Z" decreases whereas the peak frequency (ω_p) shifts to higher frequencies. For frequencies above 10^4 Hz, the curves for different bias voltages converge.

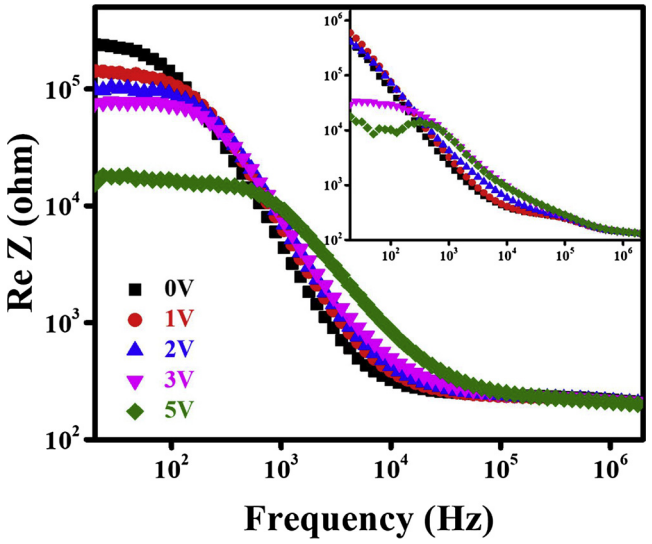

Fig. 4. Real part of impedance vs frequency (20 Hz – 2 MHz) characteristics at different bias voltages for the device D_3. Inset shows the same characteristics for the device D_0.

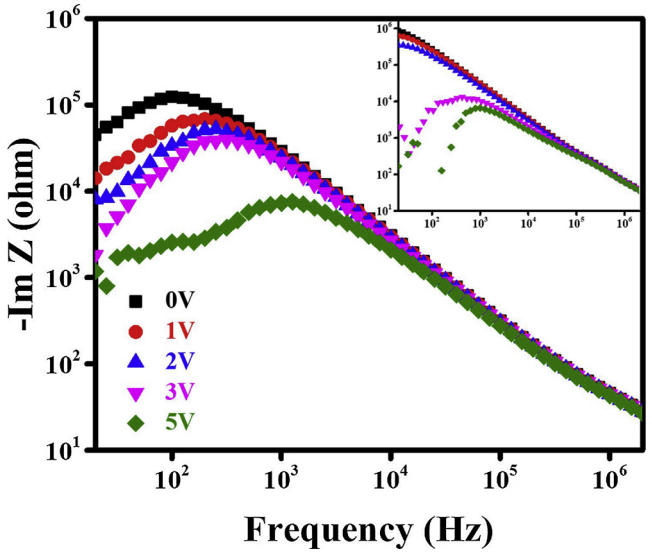

Fig. 5. Imaginary part of impedance vs frequency characteristics at different bias voltages for the device D_3. Inset shows the same characteristics for the device D_0.

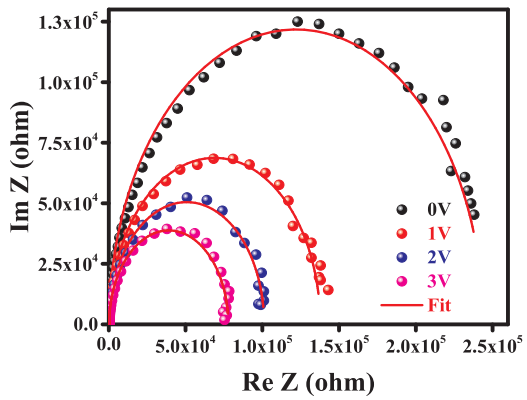

Fig. 6. Nyquist plot of the device D_3.

Table 1
Fitting parameters of impedance data for devices D_0 and D_3 at various bias voltages.

Device	D_0			D_3		
Voltage	R_s in Ω	R_p in kΩ	C_p in nF	R_s in Ω	R_p in kΩ	C_p in nF
0V	183.2	1938.0	4.60	229.50	243.50	5.26
1V	182.9	1127.0	4.62	224.50	137.50	5.34
2V	198.6	607.7	5.34	226.30	100.90	5.60
3 V	210.7	28.72	5.87	233.50	77.57	5.89

The imaginary versus the real part of the impedance generally known as the Nyquist plot and is shown in Fig. 6 for the device D_3 for different bias voltages. Each plot yields a single semicircle which corresponds to a single relaxation process. As the voltage increases, the radius of the corresponding semicircle decreases. The impedance data are fitted with the equivalent circuit model using the ZSimpWin 3.21 software. Nyquist plot for the device D_0 is shown in the supporting information. The fitting parameters of the device D_0 and D_3 are tabulated in Table. 1.

The fitting parameters and Nyquist plot for the device D_1 are given in the supporting information. Comparing fitting parameters of D_0, D_1 and D_3, it is clear that the minimum parallel resistance (R_p) and parallel capacitance (C_p) at zero bias voltage are obtained for 1:3 blend ratio of MEH-PPV:BT.

The frequency-dependent capacitance characteristics of D_0 as a function of bias voltage is shown in the inset of Fig. 7. At zero bias voltage, the capacitance is essentially equals the geometric capacitance [24], $C_0 = \varepsilon_r\varepsilon_0 A/d$, where ε_r, ε_0, A and d, are dielectric constant of the polymer, permittivity of free space, area of the device and thickness of the polymer film, respectively. At a finite bias, a negative contribution to the capacitance appears for device D_0, shifting to higher frequencies with increase in bias voltage. This negative capacitance (NC) can be attributed to the trap-assisted non-radiative recombination, a competing mechanism to bimolecular Langevin recombination [19].

The frequency-dependent capacitance of the blend device D_3 is shown in Fig. 7. The blended PLEDs have shown a different capacitance behavior at low frequencies, showing only positive capacitance values. The capacitance increases at low frequencies as the bias voltage is increased for the blended PLEDs. This increase in capacitance at low frequencies has been attributed to trapping of injected charge-carriers in distributed localized states [14]. The absence of negative capacitance at low frequencies in blended PLEDs is a clear indication of the

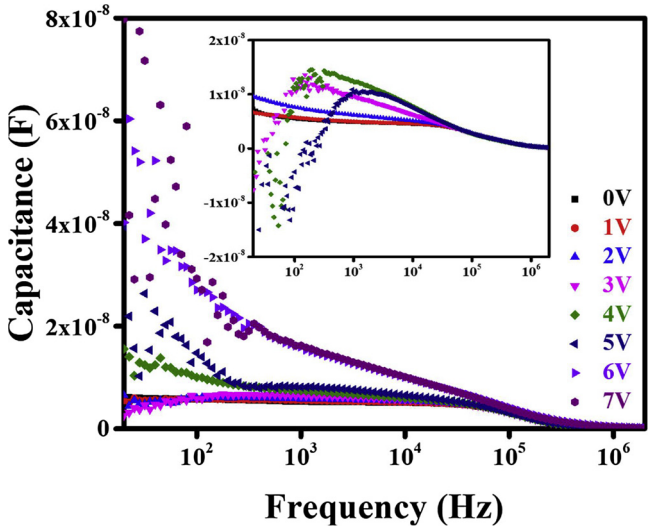

Fig. 7. Frequency-dependent capacitance (C-f) of the device D_3 as a function of bias voltage. Inset shows the same characteristics for the device D_0.

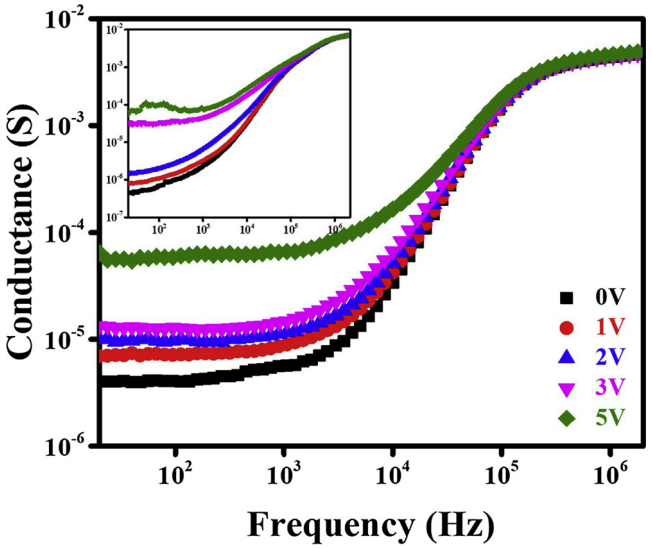

Fig. 8. Conductance vs Frequency (G-f) characteristics of the device D_3. Inset shows the same characteristics for the device D_0.

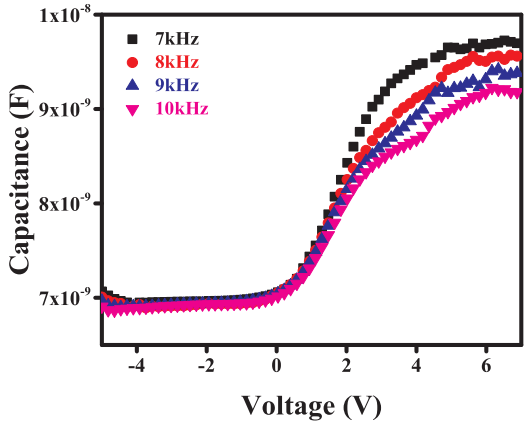

Fig. 9. Capacitance-voltage (C-V) characteristics of the device D_3 at different frequencies.

suppression of trap-assisted non-radiative recombination and leads to improved efficiency and performance of the PLEDs. These results are in accordance with the findings by Abbaszadeh et al. (2016) wherein the electron traps were effectively eliminated by blending the active semiconductor material with a large bandgap host material [25].

The frequency dependence of conductance at different bias voltages for device D_3 is shown in Fig. 8. It is evident from the graph that the conductance remains practically constant 10^{-5} S at frequencies up to 1 kHz, increases in the frequency range above 1 kHz up to about 500 kHz and finally converges to a single curve at higher frequencies. The dc conductance increases with the bias voltage and is constant at higher frequencies. The same curves for the device D_1 are shown in the supporting information. It is evident from the conductance characteristics of all the devices that blending significantly improved the conductivity at small bias voltages (< 3 V) for the blended devices compared to the unblended device D_0. This can be explained by the formation of an electron transport sub-network in MEH-PPV by blending with BT [20]. Therefore, the blend of MEH-PPV and BT at 1:3 ratio can be employed as an active material with enhanced charge carrier transport in single layer PLEDs.

The capacitance-voltage (C-V) characteristics of device D_3 at different frequencies are shown in Fig. 9. The C-V behavior is identical for all the frequencies. The capacitance is constant and independent of voltage at reverse bias because of the widening of the depletion layer. The constant capacitance at zero bias generally is described as the geometric capacitance and is seen to be 7 nF for device D_3. The capacitance increases at smaller forward bias due to injection of charge carriers. At high forward bias, capacitance decreases due to the charge carrier recombination. The charge carrier recombination is evident from the orange-red emission of the devices. For the same device, the capacitance peak value is decreased as the measurement frequency increases. The peak at higher bias voltages can be attributed to the deep traps present at the metal/organic and organic/organic interfaces [26].

4. Conclusions

It is clear that blending MEH-PPV and BT together for use as single active layer significantly decreases the turn-on voltage of the blend PLEDs. The negative capacitance seen at low frequencies in unblended MEH-PPV devices is eliminated by blending MEH-PPV with BT for use in the PLEDs. The trap-assisted recombination, a non-radiative recombination mechanism competing with the radiative Langevin recombination, is suppressed in the blended polymer devices. Moreover, the blended devices have shown considerable increase in the conductivity at small bias voltages. These results can significantly improve the performance and efficiency of the PLEDs.

Acknowledgements

A portion of this research was performed using facilities at CeNSE, funded by Ministry of Electronics and Information technology (MeitY), Govt. of India, and located at the Indian Institute of Science, Bengaluru. P.P.D. acknowledges financial support from SERB-DST, Government of India through grant award EMR/2016/000808. KMN is grateful to NITK Surathkal for providing the research fellowship.

Appendix A. Supplementary data

Supplementary material related to this article can be found, in the online version, at doi:https://doi.org/10.1016/j.synthmet.2019.03.009.

References

[1] J.H. Burroughes, et al., Light-emitting diodes based on conjugated polymers, Nature 347 (1990) 539–541.
[2] R.H. Friend, et al., Electroluminescence in conjugated polymers, Nature 397 (1999) 121–128.
[3] G. Li, R. Zhu, Y. Yang, Polymer solar cells, Nat. Photonics 6 (2012) 153–161.
[4] H. Sirringhaus, 25th anniversary article: organic field-effect transistors: the path beyond amorphous silicon, Adv. Mater. 26 (2014) 1319–1335.
[5] M.S. White, et al., Ultrathin, highly flexible and stretchable PLEDs, Nat. Photonics 7 (2013) 811–816.
[6] L. Ying, C.L. Ho, H. Wu, Y. Cao, W.Y. Wong, White polymer light-emitting devices for solid-state lighting: materials, devices, and recent progress, Adv. Mater. 26 (2014) 2459–2473.
[7] H. Zheng, et al., All-solution processed polymer light-emitting diode displays, Nat. Commun. 4 (2013) 1971.
[8] S. Reineke, et al., White organic light-emitting diodes with fluorescent tube efficiency, Nature 459 (2009) 234–238.
[9] M. Kuik, et al., 25th anniversary article: charge transport and recombination in polymer light-emitting diodes, Adv. Mater. 26 (2014) 512–531.
[10] A. Kokil, K. Yang, J. Kumar, Techniques for characterization of charge carrier mobility in organic semiconductors, J. Polym. Sci. Sci. 50 (2012) 1130–1144.
[11] Biswajit Ray, Aditya G. Baradwaj, Bryan W. Boudouris, Muhammad A. Alam, Defect characterization in organic semiconductors by forward bias capacitance – voltage (FB-CV) analysis, J. Phys. Chem. C 118 (2014) 17461–17466.
[12] J.W. Zhang, et al., Study on the basic capacitance-voltage characteristics of organic molecular semiconductors, Org. Electron. 21 (2015) 73–77.
[13] J.W. Zhang, J.J. Qin, H.M. Yu, X.Q. Chen, X.Y. Hou, Two-peak capacitance-voltage behavior in devices based on electron transport materials, Org. Electron. 28 (2016) 239–243.
[14] S. Ishihara, H. Hase, T. Okachi, H. Naito, Demonstration of determination of electron and hole drift-mobilities in organic thin films by means of impedance spectroscopy measurements, Thin Solid Films 554 (2014) 213–217.
[15] S.W. Tsang, S.K. So, J.B. Xu, Application of admittance spectroscopy to evaluate carrier mobility in organic charge transport materials, J. Appl. Phys. 99 (2006)

013706-1–7.
[16] S. Nowy, W. Ren, A. Elschner, W. Lövenich, W. Brütting, Impedance spectroscopy as a probe for the degradation of organic light-emitting diodes, J. Appl. Phys. 107 (2010) 1–10.
[17] Okachi, Nagase, Kobayashi, Naito, Determination of localized-state distributions in organic light-emitting diodes by impedance spectroscopy, Appl. Phys. Lett. 94 (2009) 43301.
[18] H.C.F. Martens, J.N. Huiberts, P.W.M. Blom, Simultaneous measurement of electron and hole mobilities in polymer light-emitting diodes, Appl. Phys. Lett. 77 (2000) 1852.
[19] Q. Niu, N.I. Crăciun, G.J.A.H. Wetzelaer, P.W.M. Blom, Origin of negative capacitance in bipolar organic diodes, Phys. Rev. Lett. 120 (2018) 1–5.
[20] M.M. Bidgoli, M. Mohsennia, F.A. Boroumand, A.M. Nia, Optoelectronic characteristics of MEH-PPV + BT blend thin films in polymer light emitting diodes, Semicond. Sci. Technol. 30 (2015) 065016.
[21] M. Mohsennia, M.M. Bidgoli, F.A. Boroumand, A.M. Nia, Electrically conductive polyaniline as hole-injection layer for MEH-PPV:BT based polymer light emitting diodes, Mater. Sci. Eng. B 197 (2015) 25–30.
[22] K.M. Nimith, M.N. Satyanarayan, G. Umesh, Enhancement in fluorescence quantum yield of MEH-PPV : BT blends for polymer light emitting diode applications, Opt. Mater. (Amst) 80 (2018) 143–148.
[23] S.H. Kim, K. Choi, H. Lee, D. Hwang, L. Do, Impedance spectroscopy of single- and double-layer polymer light-emitting diode, J. Appl. Phys. 87 (2000) 882–888.
[24] V. Shrotriya, Y. Yang, Capacitance-voltage characterization of polymer light-emitting diodes, J. Appl. Phys. 97 (2005) 1–6.
[25] D. Abbaszadeh, et al., Elimination of charge carrier trapping in diluted semiconductors, Nat. Mater. 15 (2016) 628–633.
[26] A. Sharma, P. Kumar, B. Singh, S.R. Chaudhuri, S. Ghosh, Capacitance-voltage characteristics of organic schottky diode with and without deep traps, Appl. Phys. Lett. 99 (2011) 023301.

Journal of Photochemistry & Photobiology A: Chemistry 378 (2019) 38–45

Contents lists available at ScienceDirect

Journal of Photochemistry & Photobiology A: Chemistry

journal homepage: www.elsevier.com/locate/jphotochem

New blue light emitting cyanopyridine based conjugated polymers: From molecular engineering to PLED applications

Naveenchandra Pilicode[a], Nimith K. M[b], Madhukara Acharya[a], Praveen Naik[a], Satyanarayan M. N[b], Airody Vasudeva Adhikari[a,*]

[a] Organic Materials Laboratory, Department of Chemistry, National Institute of Technology Karnataka, Surathkal, Mangalore, 575 025, India
[b] Department of Physics, National Institute of Technology Karnataka, Surathkal, Mangalore, 575 025, India

ARTICLE INFO

Keywords:
Auxiliary donors
Blue light emitter
Cyanopyridine
Conjugated polymers
PLED

ABSTRACT

In this work, we report the design of three new cyanopyridine scaffold based polymers, *viz*. **TPy$_{1-3}$** as potential blue light emitters for PLED applications. The new polymer design comprise, a cyanopyridine core as an electron accepting entity, thiophene as an electron donating unit with different auxiliary donors, *viz.* phenylene (**TPy$_1$**), biphenyl (**TPy$_2$**), and fluorene (**TPy$_3$**), and have been synthesized, following standard synthetic protocols including Suzuki-cross coupling polymerization reaction. Further, in order to assess all the prerequisites to act as an active emitter, the polymers **TPy$_{1-3}$**, were subjected to structural, thermal, linear optical, electrochemical and computational studies. The results revealed that, all the polymers were thermally stable up to 300 ^{0}C and their estimated optical band-gaps were found to be 2.59–2.80 eV. Finally, new polymer light emitting diode (PLED) were fabricated by employing the polymers **TPy$_{1-3}$**, as active emissive material with a configuration of ITO/PEDOT: PSS/Polymer/Al. Interestingly, all the fabricated devices, exhibited an intense blue electroluminescence at 12 V with low threshold voltages of 4.2–4.8 V, signifying an effective injection of electron in the device.

1. Introduction

Over the past few decades, PLEDs have gained substantial attention in the field of optoelectronics due to their cost-effective, light weight and ease of fabrication [1–4]. In PLED devices, photo functional conjugated polymers are considered to be prospective candidates as emitters due to their several advantages such as design versatility, tunable optical and electrochemical properties, good processability, low operating voltage and high flexibility, over the inorganic or organic small molecules [5,6]. Basically, such polymers comprise of a rigid backbone scaffold along with both electron rich donating and electron-deficient accepting moieties to facilitate optimum electron injection and transport, providing better charge carrier balance in the device [7,8]. Amongst them, the conjugated polymers carrying N-heterocyclic moieties have attracted significant interest as emitters in PLED devices, mainly due to their high electron-accepting abilities, good charge injection and excellent thermal as well as oxidation stability [9,10].

Recently, polymers centered on cyanopyridine core are being investigated widely for various optoelectronic applications owing to their high electron carrying ability as well as excellent fluorescence property [11]. Further, their photophysical behavior can be tuned easily by incorporating various electron donor/π-spacer functionalities in the polymer backbone [12]. Additionally, the inclusion of long chain alkoxy group to cyanopyridine scaffold would increase the polymer's solubility and film forming ability of polyme [13,14]. Also, it is well-documented that, the presence of highly stable thiophene ring in the conjugated polymer chain, leads to improvement in chemical stability and hole transporting ability of the polymers [15]. In fact, the high polarizability of sulphur (S) atom in thiophene stabilizes the macromolecule and improves charge transport behavior [16,17]. Moreover, in the literature, benzene and its derivatives have been effectively utilized as π conjugation linkers in conjugated polymers due to their electrochemical and thermal stability, tunable spectroscopic and electrochemical characteristics and good charge transporting ability [18]. Also, it is well-established that, fluorene and its derivatives are attractive materials mainly ascribed to their good stability (both thermal and chemical) and extremely high fluorescence quantum yields [19–22].

Against this background, in the present work, a new series of 2-hexadecoxylcyanopyridine based polymers, **TPy$_{1-3}$** carrying thiophene rings was designed. The new design includes phenylene (**TPy$_1$**), biphenyl (**TPy$_2$**) and fluorene (**TPy$_3$**) moieties as π-conjugated auxiliary donors in the main chain primarily for enhancing the electrochemical

* Corresponding author.
E-mail address: avachem@gmail.com (A.V. Adhikari).

https://doi.org/10.1016/j.jphotochem.2019.04.012
Received 10 February 2019; Received in revised form 6 April 2019; Accepted 9 April 2019
Available online 10 April 2019

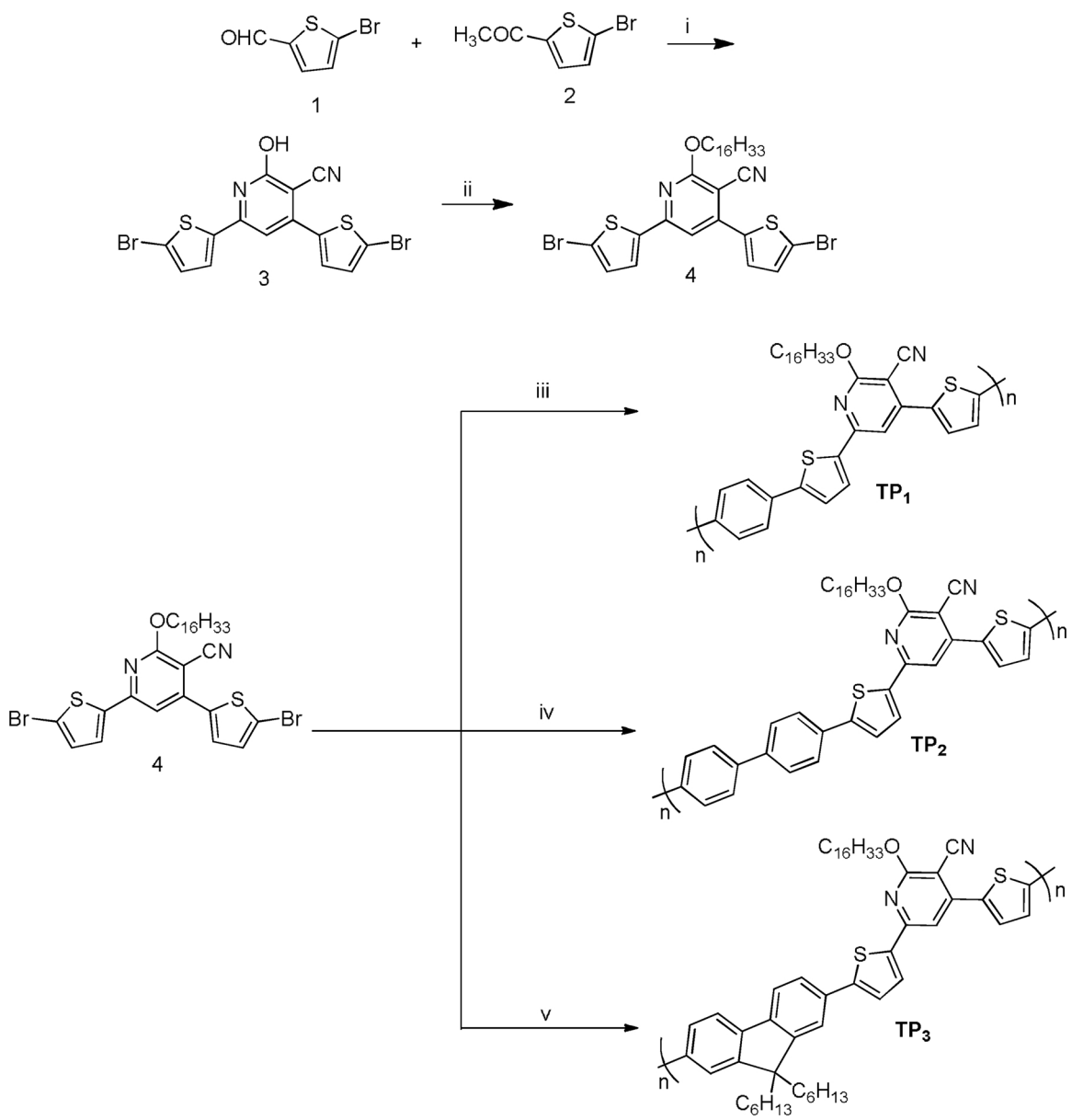

Scheme 1. Synthetic pathways of new polymers **TPy$_{1\text{-}3}$**. Reaction conditions: (i) $CNCH_2COOC_2H_5$, CH_3COONH_4, 1,4-dioxane, 80 °C, 24 h; (ii) 1-bromohexadecane, K_2CO_3, DMF, 80 ^{0}C, 9 h; (iii) 1,4-phenylenebisboronic acid, $Pd(PPh_3)_4$, toluene-ethanol (1:1), Cs_2CO_3, 90 ^{0}C, 12 h; (iii) 4,4′-biphenyldiboronic acid, $Pd(PPh_3)_4$, toluene-ethanol (1:1), Cs_2CO_3, 90 ^{0}C, 12 h; (iii) 9,9-dihexylfluorene-2,7-diboronic acid, $Pd(PPh_3)_4$, toluene-ethanol (1:1), Cs_2CO_3, 90 ^{0}C, 15 h.

and optical properties as well as the overall stability and rigidity of resulting polymers. Here, cyanopyridine core being a strong electron acceptor, facilitates good charge transporting behavior, while thiophene rings on either side of cyanopyridine core act as strong electron donors. Further, presence of bulky alkoxy chain would bring good solubility as well as film forming nature of the polymers. The newly designed polymers were expected to own desired properties such as high molecular weight with great degree of solubility in common organic solvents, attractive charge carrying ability, good thermal stability, wide band gap, excellent quantum yield and blue fluorescence. The target polymers were synthesized from simple thiophene derivatives using standard synthetic protocols. We have employed the Suzuki cross-coupling method for the polycondensation of the cyanopyridines to achieve high molecular weight and low polydispersity index in the target polymers. However, there are no reports available in the literature on polymerization of cyanopyridine derivatives by Suzuki technique.

The new polymers and their intermediates were characterized using NMR, FTIR spectral and elemental analysis. Their weight average molecular mass ($\overline{M}_w$) along with polydispersity index (PDI) were determined from Gel permeation chromatography (GPC) technique. Their thermal stability with respect to temperature was investigated by the thermo gravimetric analysis (TGA). Further, their photophysical properties in both solution as well as solid film were studied by employing UV–vis. absorption as well PL emission spectroscopy. In addition, their HOMO-LUMO energy levels were determined using both spectral as well as cyclic voltammetric (CV) method. Further, DFT (density functional theory) studies were performed on the newly synthesized polymer, by considering the repeating units (monomers) at B3LYP/TZVP level using Tmolex. Finally, light emitting nature of newly synthesized polymers was determined by fabricating LED devices. The device was fabricated with the configuration, ITO/PEDOT: PSS/Polymer/Al, where the polymer functions as a light emissive layer in their respective device. In addition, the polymer structure and its effect on the various properties have been well explained.

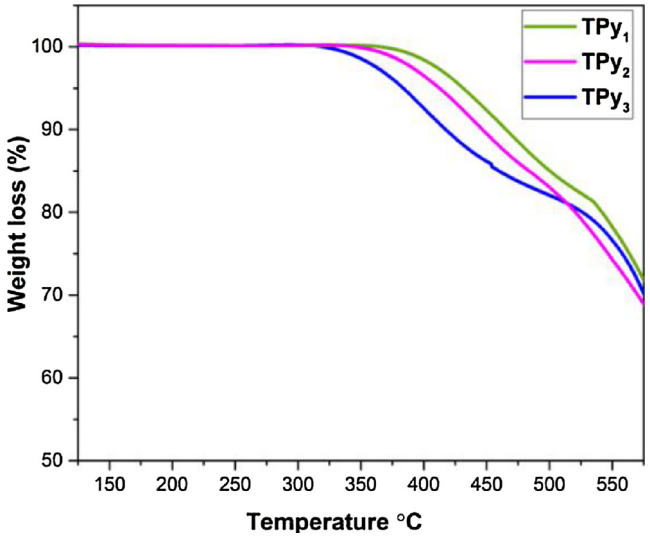

Fig. 1. TGA traces of **TPy$_{1\text{-}3}$**.

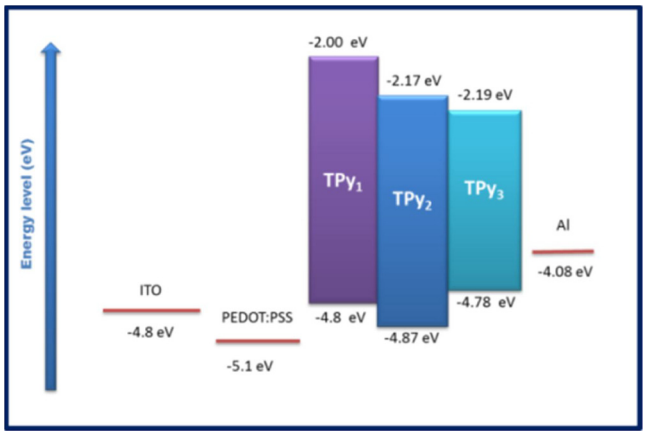

Fig. 2. Energy band diagram of **TPy$_{1\text{-}3}$** based device.

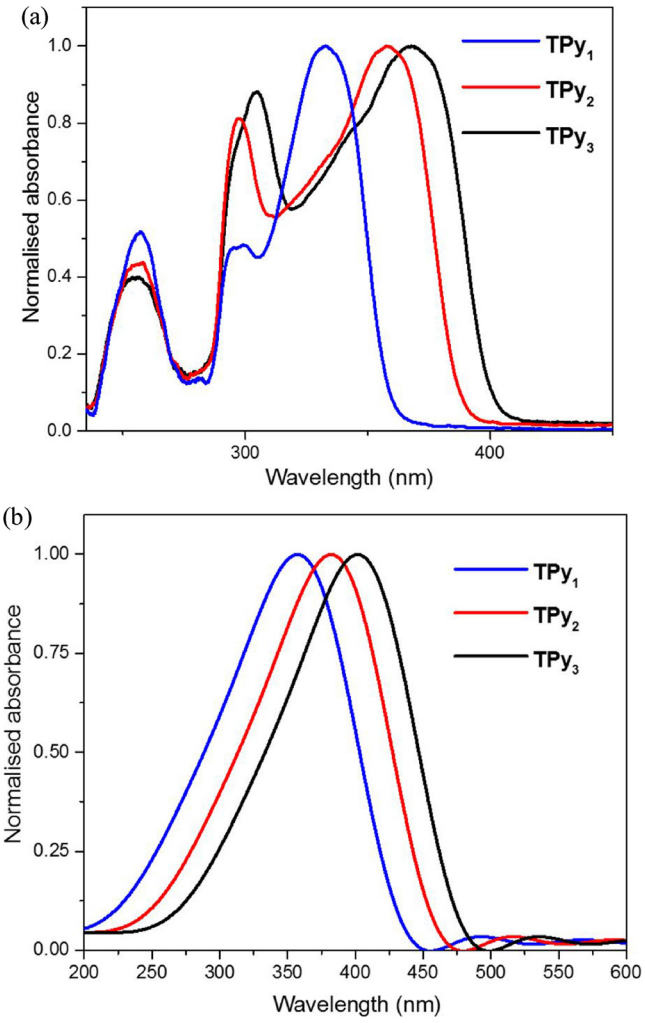

Fig. 3. (a) UV–vis spectra of polymers **TPy$_{1\text{-}3}$** in THF (10^{-6} M conc.) solution. (b) UV–vis spectra of polymers **TPy$_{1\text{-}3}$** in solid film state.

2. Experimental

2.1. Materials and measurements

All the required chemicals are procured from companies such as Alfa Aesar, Sigma Aldrich, Spectrochem and TCI India. All the solvents used in the reaction were of synthetic grade and used without any further purification. The reaction progress was monitored by Thin Layer Chromatography (TLC) technique. The purification of monomer as well as its intermediate was done by column chromatography (100–200 mesh silica) and recrystallization techniques, respectively. The synthesized polymers **TPy$_{1\text{-}3}$**, were purified by Soxhlet extraction technique followed by re-precipitation method.

The FTIR (Bruker Alpha), ^{1}H NMR (Bruker Avance 300 MHz) and CHN analyzer (Thermo Fischer Flash EA1112) were used for the structural elucidation of new molecules. Further, Ultraviolet-Visible (UV–vis.) absorption and photoluminance (PL) emission spectra of the polymers **TPy$_{1\text{-}3}$** using SPECORD S600 and Horiba Fluromax-4 spectrophotometers respectively. Furthermore, the cyclic voltammetric (CV) measurements were carried out using Ivium Vertex electrochemical workstation. Moreover, the $\overline{M}_w$ of polymers was determined against polystyrene standards with THF as an eluent using WATER's make GPC system. Finally, DFT calculations were executed for the repeating units of polymers **TPy$_{1\text{-}3}$**, by using Turbomole-7.2 V software.

Table 1
Photophysical and electrochemical data of **TPy$_{1\text{-}3}$**.

Polymer		TPy$_1$	TPy$_2$	TPy$_3$
UV -Visible	λ^a_{max}nm	333	357	367
	λ^b_{max}nm	356	382	402
	λ^b_{onset}nm	434	459	478
Fluorescence	λ^a_{em}nm	378	405	419
	λ^b_{em}nm	418	432	441
E_g^{opt}**eV**		2.80	2.70	2.59
E_g^{DFT}**eV**		3.30	3.14	3.31
LUMO (CV) eV		–2.00	–2.17	–2.19
LUMO (DFT) eV		–2.64	–2.42	–2.45
HOMO eV		–4.80	–4.87	–4.78
HOMO (DFT) eV		–5.94	–5.56	–5.76
Stoke Shift cm^{-1}		3575	3320	3380
Φ_f (%)		35.47	39.12	48.32
ε(M^{-1} cm^{-1}) at λ^a_{max}		14,492 (360 nm)	15,258 (357 nm)	18,866 (367 nm)

a Polymer solution state.
b Polymer film state.
Φ_f: Fluorescence quantum yield.
ε : Molar absorption coefficient.

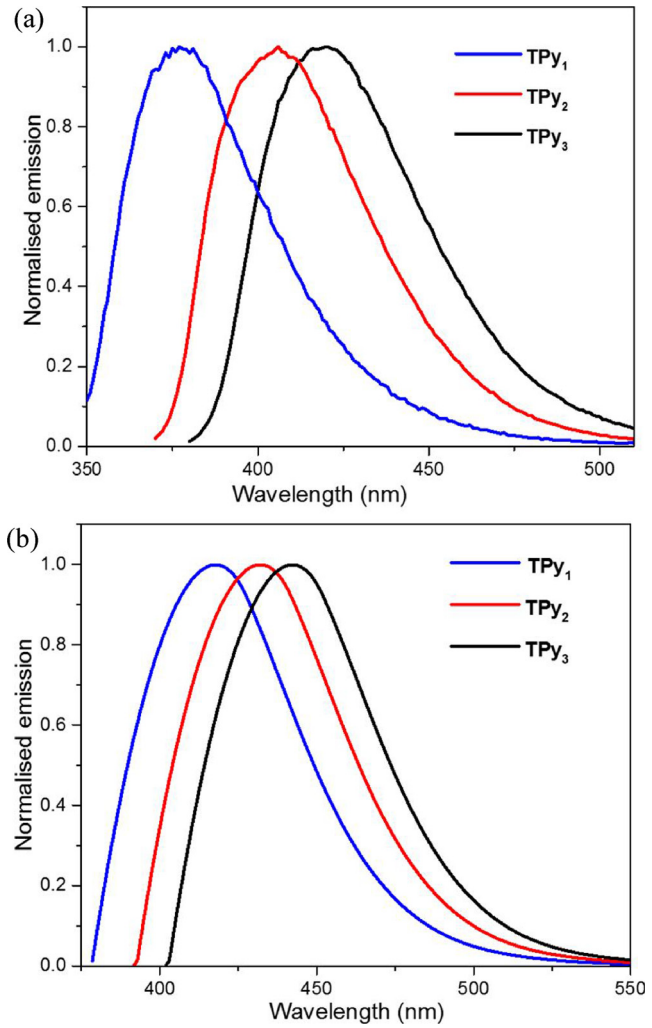

Fig. 4. (a) PL emission spectra of polymers $\mathbf{TPy_{1\text{-}3}}$ in THF (10^{-6} M conc.) solution. (b) PL emission spectra of polymers $\mathbf{TPy_{1\text{-}3}}$, in solid film state.

2.2. Synthesis

2.2.1. Synthesis of intermediate (3) and monomer (4)

The key intermediate **3** and cyanopyridine monomer **4** were synthesized as per reported procedure [23].

2.2.2. General synthesis of the polymer ($TPy_{1\text{-}3}$)

A mixture of cyanopyridine based monomer (**4,** 1 g, 1.5 mmol), Cs_2CO_3 (3.4 g, 10.5 mmol), and $Pd(PPh_3)_4$ (0.84 g, 0.75 mmol) in 20 mL of dried 1:1 mixture toluene and ethanol mixture was taken in 100 mL two neck round bottom flask. To above mixture, 1.5 mmol of respective boronic acid *Viz.* 1,4-phenylenebisboronic acid (***TPy₁***), 4,4′-biphenyldiboronic acid (***TPy₂***) and 9,9-dihexylfluorene-2,7-diboronic acid (***TPy₃***) were added and refluxed under argon atmosphere. The reaction mixture was cooled down to room temperature, excess solvent was removed under reduced pressure. The obtained reaction mass was further dissolved in CH_2Cl_2 and filtered using the Celite bed to remove catalytic traces. The obtained filtrate was thoroughly washed with distilled water to remove traces of solvent and base. Then the solvent in the organic layer was removed under the vacuum. Further, to remove the lower weight oligomer fractions, the resultant crude product was subjected to Soxhlet extraction using solvents like methanol, acetone, and hexane. Finally, the crude product was dissolved in limited amount of chloroform, followed by re-precipitation using methanol to get the pure polymer.

TPy₁: Fluorescent yellowish color solid, Yield 65%. FTIR (cm^{-1}): 2221 (-C≡N), 2918 (-C-H). ^{1}H NMR (300 MHz, $CDCl_3$, δ ppm): 0.89–1.88 (m, 31 H), 4.55–4.61 (b, 2 H), 7.39–7.70 (m, 9 H). $\overline{M}_w$, 33,164 g/mol, PDI, 1.23. CHN, calculated: C, 74.46; H, 7.89; N, 4.57; found: C, 74.44; H, 7.88; N, 4.55.

TPy₂: Pale yellow color solid, Yield 68%. FTIR (cm^{-1}): 2218 (C≡N), 2918 (C–H). ^{1}H NMR (300 MHz, $CDCl_3$, δ ppm): 0.89–1.88 (m, 31 H), 4.56–4.61 (b, 2 H), 7.39–7.71 (m, 13 H). $\overline{M}_w$, 45,127 g/mol, PDI, 1.24. CHN, calculated.: C, 76.70; H, 7.61; N, 4.07; found: C, 76.69; H, 7.60; N, 4.06.

TPy₃: whitish yellow powder, Yield 69%. FTIR (cm^{-1}): 2212 (C≡N), 2918 (C–H). ^{1}H NMR (300 MHz, $CDCl_3$, δ ppm): 0.89–1.95 (m, 43 H), 4.48–4.62 (b, 6 H), 7.52–8.05 (m, 11 H). $\overline{M}_w$, 52,763 g/mol, PDI, 1.21. CHN calculated for $\mathbf{TPy_3}$: C, 78.75; H, 8.81; N, 3.22; found: C, 78.74; H, 8.80; N, 3.21.

3. Results and discussion

3.1. Synthesis of polymers $TPy_{1\text{-}3}$

The employed synthetic pathways for the preparation of the desired new intermediate/monomer as well as polymers are represented in Scheme 1. Initially, cyanopyridine intermediate (**3**) was synthesized from the 5-bromo-thiophene-2-carboxaldehyde (**1**) condensing with 2-acetyl-5-bromothiophene (**2**). Further, the intermediate **3** was O-alkylated using n-bromohexadecane to yield 2-hexadecylcyanopyridine (**4**). Furthermore, the targeted new polymers $\mathbf{TPy_{1\text{-}3}}$ was obtained in good yield following renowned Suzuki coupling polymerization reaction, under anhydrous condition. Their chemical structures were well established using FTIR, ^{1}H NMR spectral and elemental analysis. Finally, all the polymers $\mathbf{TPy_{1\text{-}3}}$ was subjected to GPC technique for determining $\overline{M}_w$ and polydispersity of $\mathbf{TPy_{1\text{-}3}}$. The GPC results revealed that, they have $\overline{M}_w$ of 33,164, 45,127 and 52,763 g/mol, respectively and the polydispersity were in the order of 1.23, 1.24 and 1.21, respectively.

3.2. Solubility of polymers

The solubility of new polymers $\mathbf{TPy_{1\text{-}3}}$ was tested in organic solvents *Viz.* tetrahydrofuran (THF), dichloromethane (DCM), chloroform ($CHCl_3$), and dimethyl sulfoxide (DMSO). They displayed better solubility in aforementioned solvents, which can be ascribed to the bulkier hexadecoxyl alkyl chain present on cyanopyridine core. Hence all the synthesized polymers $\mathbf{TPy_{1\text{-}3}}$, displayed good processability along with film forming nature. Amongst them, $\mathbf{TPy_3}$ was found to show the highest solubility and good film forming ability due to presence of dihexyl fluorene units along with hexadecoxylcyanopyridine in polymer main chain.

3.3. Thermal analysis

In order to access the thermal stability of the synthesized polymers $\mathbf{TPy_{1\text{-}3}}$, the TGA investigation were carried out in a nitrogen atmosphere by temperature ramp of 10 ^{0}C min^{-1} ranging from 50 to 600 ^{0}C. Their thermograms are depicted in Fig. 1 and the thermal degradation temperatures of $\mathbf{TPy_1}$, $\mathbf{TPy_2}$ and $\mathbf{TPy_3}$, were found to be 367, 351 and 318 ^{0}C, respectively. Interestingly, all the polymers $\mathbf{TPy_{1\text{-}3}}$, demonstrated a high degree of thermal stability can be attributed to the presence of rigid aromatic heterocyclic ring systems in the polymer. Further, at 300 ^{0}C, about 20–25% of weight loss was observed mainly due to the degradation of the hexadecoxyl alkyl chain on the cyanopyridine scaffold. Finally, a gradual loss in weight was observed over 350 ^{0}C, which can be attributed to the further degradation of the macromolecular chain, which results in residue formation. Similar results were made for cyanopyridne based conjugated polymers reported earlier [23–25].

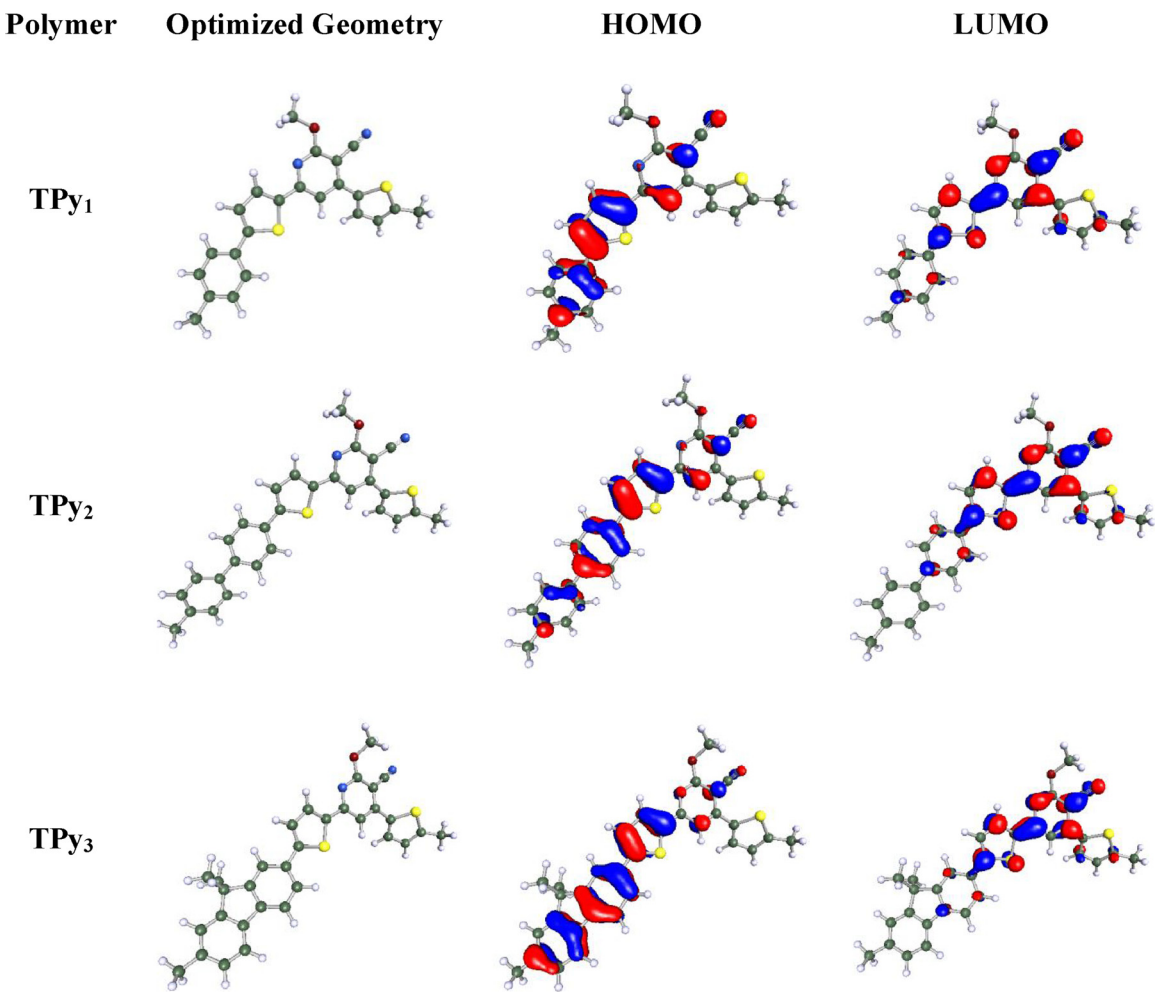

Fig. 5. Structurally optimized geometries along with simulated FMO levels of **TPy$_{1\text{-}3}$**.

3.4. Electrochemical studies

The electrochemical properties such as charge carrying and energy distributed in the FMO (Frontier molecular orbital) levels of polymers **TPy$_{1\text{-}3}$**, were investigated by CV measurements. In the current work, the cyclic voltamograms for polymer were recorded using standard three electrode system, consisting a working electrode (polymer coated on glassy carbon electrode), a reference electrode usually Ag/AgCl and a counter electrode (Pt electrode). These three electrodes were dipped in acetonitrile solution consisting of an electrolyte [0.1 M $(n\text{-}Bu)_4N^+PF_6^-$] and CV data were recorded at a scan rate of 100 mV/s. The resultant CV traces of **TPy$_{1\text{-}3}$** were given in ESI (electronic supplementary information). From the results, it is quite evident that, the only reduction potential for **TPy$_{1\text{-}3}$** were observed, which are in agreement with previously reported cyanopyridine based conjugated polymers [23].

The LUMO (Lowest unoccupied molecular orbital) energy levels of the **TPy$_{1\text{-}3}$** were calculated by substituting the reduction potential value obtained from the CV traces into the equation: $E_{LUMO} = -e[E_{red} + 4.8 - E_{FOC}]$ [25]. Hence, the LUMO energy levels for **TPy$_{1\text{-}3}$** and were estimated to be –2.00, –2.17 and –2.19 eV, respectively. Since CV traces of **TPy$_{1\text{-}3}$** showed no oxidation potentials, the required HOMO (Highest occupied molecular orbital) levels were determined from their optical energy band gap. Thus, the HOMO energy levels for **TPy$_{1\text{-}3}$** were found to be –4.8, –4.87 and –4.78 eV, respectively. Fig. 2 envisages energy level diagram of **TPy$_{1\text{-}3}$**, wherein FMO energy levels of polymers were compared with work functions of ITO and aluminum along with energy levels of hole injecting layer PEDOT:PSS of the PLED device.

3.5. Photophysical properties

The UV–vis, absorption spectra of polymers **TPy$_{1\text{-}3}$**, recorded in THF (10^{-6} M conc) solution and thin coated solid film, respectively were portrayed in the Fig. 3**(a–b)** and their pertaining spectral data were tabulated in Table 1. The absorption maxima λ_{max} obtained in solution state was found to be 333, 357 and 367 nm, where as a slightly red shifted absorption of 356, 382 and 402 nm were observed in thin film state, respectively. However, the observed red shift of about 23 nm (**TPy$_1$**), 25 nm (**TPy$_2$**) and 35 nm (**TPy$_3$**) in the absorption spectra confirms the effect of inter-chain interaction and inter-chain mobility of the excitons and excimers generated within the conjugated polymer in solid film state [23]. In addition, a small absorption maxima observed at lower energy level of film state can be attributed to the presence of trace of cyanopyridine monomer impurity trapped inside polymer chain. Moreover, the obtained results revealed that, the polymers **TPy$_{1\text{-}3}$**, displayed similar electronic behaviors both in solution as well in thin film states. Furthermore, their optical energy band gaps were calculated from the onset absorption edge λ^b_{onset} of UV–vis. spectra obtained from thin film (Fig. 3**b**) [17]. Consequently, their optical energy band gap was found to be in the decreasing order of **TPy$_1$** (2.80 eV) > **TPy$_2$** (2.70 eV) > **TPy$_3$** (2.59 eV). Typically, the polymers with wide energy band gap are highly preferred in blue light PLED applications. Finally, their molar extinction coefficients **(ε)** was determined by using Beer-Lambert law, and found to be 14,492 M^{-1} cm^{-1} (**TPy$_1$**), 15,258 M^{-1} cm^{-1} (**TPy$_2$**) and 18,866 M^{-1} cm^{-1}(**TPy$_3$**), respectively.

Fig. 4**a** and **b**, showcase the PL emission spectra of **TPy$_{1\text{-}3}$** recorded at their respective excitation wavelengths in THF (10^{-6} M conc.)

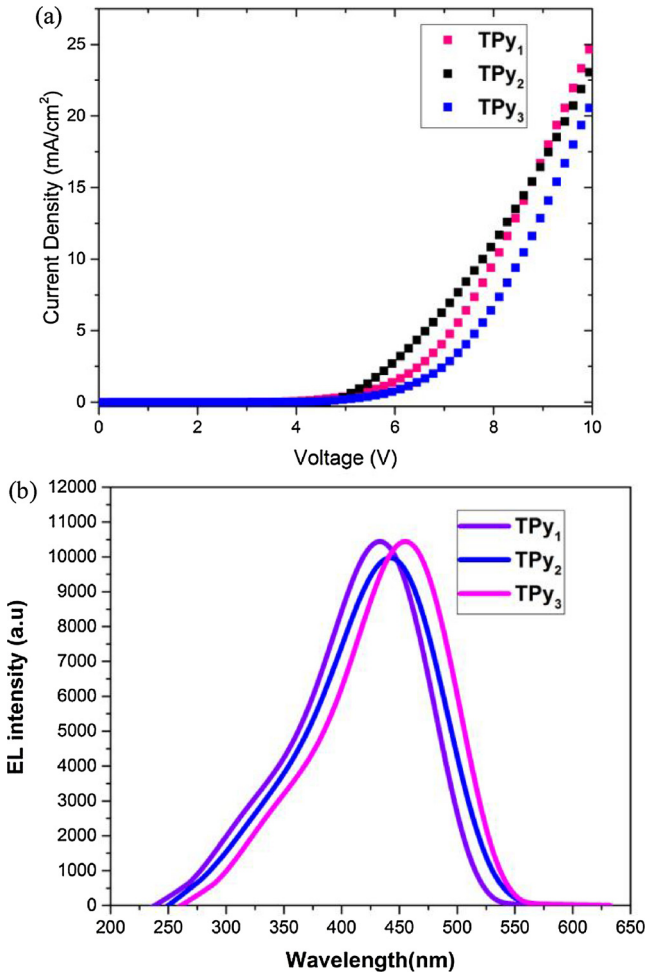

Fig. 6. (a) *J-V* curves of PLED device. (b) EL of **TPy$_{1\text{-}3}$** at driving voltage of 12V.

solution and spin coated polymer film state, respectively, and their resultant spectral data are given in Table 1. From the Fig. 4**a-b**, it is clear that, the polymers displayed intense emission bands λ_{em} in THF solution at 378, 405, and 419 nm, while, in the thiln film, λ_{em} was slightly red shifted to 418, 432 and 441 nm, respectively. This can be attributed to the π–π* stacking of polymer chains in thin films. Further, the Stoke shifts of **TPy$_{1\text{-}3}$** were calculated from the difference between the absorption maxima (λ_{max}) and emission maxima (λ_{em}) values obtained in solution state. The calculated Stoke shifts were found to be 3575, 3320 and 3380 cm^{-1} for **TPy$_{1\text{-}3}$**, respectively. Further, fluorescence quantum yield (Φ_f) determination for polymer solution was carried out using quinine sulphate as reference standard (degassed in 0.05 M sulfuric acid, with Φ_f of 52%). The Φ_f values for **TPy$_{1\text{-}3}$**, were found to be 35.47%, 39.12% and 48.32%, respectively. The obtained results were very much comparable to the previously reported conjugated polymers based on cyanopyridine scaffold [23]. Overall, these blue light emitting polymers, **TPy$_{1\text{-}3}$**, possess fairly good Φ_f values and therefore, they can be employed as potential emitter for PLED device applications.

3.6. Computational studies

The DFT simulations were performed with Turbomole V7.2 software package to get deeper insight into the electron density distributions in their FMO energy levels as well as optimized molecular geometry of the synthesized polymers **TPy$_{1\text{-}3}$** [26,27]. In order to simplify the computational complexity, in the present work, only one repeating unit of the polymers **TPy$_{1\text{-}3}$**, were taken into the consideration and the long alkyl chain present in the repeated units were subsequently replaced by methyl ($-CH_3$). To begin with, all the structures were first optimized in the gas phase with semi-empirical Austin Model 1 AM1/COSMO in 3D molecular builder of Tmole software at the B3LYP/TZVP level.

The Fig. 5 shows the optimized molecular geometries of the repeated units of the **TPy$_{1\text{-}3}$**, along with electronic distribution in their FMO energy levels. Their theoretically estimated FMO energy levels were tabulated in Table 1. The predicted FMO energy values of the **TPy$_{1\text{-}3}$**, moderately differs from experimental values, which may be ascribed to the fact that, while performing the simulations, the various realistic phenomenon such as effect of solvent, electrolyte and conformational order in bulk state were not taken into account [28–32]. From Fig. 5 it is quite evident that, in HOMO energy levels of **TPy$_{1\text{-}3}$**, the electron density is mainly concentrated on donor part. Whereas, in LUMO levels, the electron density is mostly localized on the electron deficient cyanopyridine scaffold.

3.7. I-V characteristics and electroluminescence studies

New ITO/PEDOT: PSS/Polymer/Al configured PLED devices were fabricated using **TPy$_{1\text{-}3}$** as emissive material to study the electroluminescence (EL) characteristics. The devices fabrications was done following standard procedure and no protective encapsulation materials were used in this work [33–35]. The detailed procedure for device fabrication has been given in the ESI. Further, Figs. 6**a** and **b**, showcases the *J–V* (current-voltage) characteristic curves and EL emission spectra of the new PLED devices. Interestingly, Fig. 6**a** showed a steady rise in the current density with the increasing forward bias voltage indicating distinctive diode characteristic [36,37]. Further, the PLED devices showed low threshold voltage of 4.20, 4.55 and 4.80 eV for **TPy$_1$**, **TPy$_2$** and **TPy$_3$**, respectively, which may be due to their low LUMO energy levels, which reduces the energy barrier of electron injection from the cathode [38–42]. The observed low threshold voltages are in very much comparable with previously reported PLED device [23]. Furthermore, their EL emission maxima were found to be 476 nm (**TPy$_1$**), 469 nm (**TPy$_2$**), and 471 nm (**TPy$_3$**) at driving voltage of 12 V. From Fig. 6b, it is quite evident that, the polymers **TPy$_{1\text{-}3}$** displays a blue electroluminescence with a lower threshold voltage of 4.20–4.80 V when compare to similar reported polymers [25]. Conclusively, these cyanopyridine containing conjugated polymers as active emissive layers in the fabrication of new PLEDs has displayed better device performance when compared with that of previously reported similar type of polymers [25]. Consequently, these new polymers **TPy$_{1\text{-}3}$** are considered to be promising emitters for the applications of PLED.

4. Conclusion

Conclusively, we have successfully designed, synthesized and characterized three new cyanopyridine based conjugated polymers, **TPy$_{1\text{-}3}$** as blue light emitter. The polymers and their intermediate/monomers were synthesized by standard synthetic protocol including Suzuki cross coupling polycondensation technique. It is noteworthy that, the synthesis of **TPy$_{1\text{-}3}$** proceeds in few steps with good yields and this polymerization methodology is different from the previous study [23]. Further, the TGA studies reveal that, the polymers are thermally stable up to 318–367 ^{0}C and the photophysical data indicate that, they exhibit a wide energy bandgap of 2.59–2.8 eV. Moreover, these polymers exhibited good light absorption and blue emission in the range of 356–402 nm and 418–441 nm, respectively. Furthermore, they displayed good fluorescence quantum yields of 35–48%. Finally, the PLED devices were fabricated using this polymer as a light emissive material and the device illustrated an enhanced performance at a threshold voltage of 4.20–4.80 V, demonstrating efficiently electron injection to the device. Conclusively, from the results, it is quite evident that, the polymers **TPy$_{1\text{-}3}$**, are promising candidates as emitters for electroluminescence device applications since they possess all the required

prerequisites.

Acknowledgements

The authors express their sincere gratitude to the NITK, Surathkal, India, for providing essential laboratory and fabrication facilities for this research work. Authors thank Dr. Murali M. G., for his constant help and support. NP acknowledges Mr. Shrirang Hindalekar of BASF Innovation Campus, Mumbai, India for synthetic and analytical facilities. Also, NP indebted to Mr. Ranjit Salvi and Mr. Abhijit Vaichal of BASF India Ltd. for their motivational and administrative support.

Appendix A. Supplementary data

Supplementary material related to this article can be found, in the online version, at doi:https://doi.org/10.1016/j.jphotochem.2019.04.012.

References

[1] F. Dumur, F. Goubard, Triphenylamines and 1,3,4-oxadiazoles: a versatile combination for controlling the charge balance in organic electronics, New J. Chem. 38 (2014) 2204–2224, https://doi.org/10.1039/C3NJ01537H.
[2] J.H. Cook, J. Santos, H.A. Al-Attar, M.R. Bryce, A.P. Monkman, High brightness deep blue/violet fluorescent polymer light-emitting diodes (PLEDs), J. Mater. Chem. C 3 (2015) 9664–9669, https://doi.org/10.1039/C5TC02162F.
[3] X. Liu, X. Qi, J. Gao, S. Zou, H. Zhang, W. Hao, Z. Zang, H. Li, W. Hu, Dialkylated dibenzotetrathienoacene derivative as semiconductor for organic field effect transistors, Org. Electron. 15 (2014) 156–161, https://doi.org/10.1016/j.orgel.2013.11.016.
[4] V. Tirumalachetty, K. Palaninathan, Blue and green light emitting polyarylpyrazolines luminogens containing anthracene and thiophene units, J. Photochem. Photobiol. A 359 (2018) 64–72, https://doi.org/10.1016/j.jphotochem.2018.03.044.
[5] H. Dong, H. Zhu, Q. Meng, X. Gong, W. Hu, Organic photoresponse materials and devices, Chem. Soc. Rev. 41 (2012) 1754–1808, https://doi.org/10.1039/c1cs15205j.
[6] L. Yang, Y. Liao, J.K. Feng, A.M. Ren, Theoretical studies of the modulation of polymer electronic and optical properties through the introduction of the electron-donating 3,4-ethylenedioxythiophene or electron-accepting pyridine and 1,3,4-oxadiazole moieties, J. Phys. Chem. A 109 (2005) 7764–7774, https://doi.org/10.1021/jp0515277.
[7] A. Iqbal, S.H. Lee, O.O. Park, H.M. Siddiqi, T. Akhter, Synthesis and characterization of blue light emitting redox-active polyimides bearing a noncoplanar fused carbazole-triphenylamine unit, New J. Chem. 40 (2016) 5285–5293, https://doi.org/10.1039/c6nj00702c.
[8] X. Pan, S. Liu, H.S.O. Chan, S.C. Ng, Novel fluorescent carbazolyl-pyridinyl alternating copoloymers: synthesis, characterization, and properties, Macromolecules 38 (2005) 7629–7635, https://doi.org/10.1021/ma050425b.
[9] J. Roncali, Synthetic principles for bandgap control in linear π-Conjugated systems, Chem. Rev. 97 (1997) 173–206, https://doi.org/10.1111/j.1754-4505.2009.00107.x.
[10] R. Scaria, N.T. Lucas, K. Müllen, J. Jacob, Blue-emitting copolymers of isoquinoline and fluorene, React. Funct. Polym. 71 (2011) 849–856, https://doi.org/10.1016/j.reactfunctpolym.2011.05.006.
[11] K.L. Wang, W.T. Liou, D.J. Liaw, W.T. Chen, A novel fluorescent poly(pyridine-imide) acid chemosensor, Dyes Pigm. 78 (2008) 93–100, https://doi.org/10.1016/j.dyepig.2007.10.015.
[12] H. Wang, Z. Li, B. Huang, Z. Jiang, Y. Liang, H. Wang, J. Qin, G. Yu, Y. Liu, Y. Song, Synthesis, light-emitting and optical limiting properties of new donor-acceptor conjugated polymers derived from 3,5-dicyano-2,4,6-tristyrylpyridine, React. Funct. Polym. 66 (2006) 993–1002, https://doi.org/10.1016/j.reactfunctpolym.2006.01.008.
[13] K.L. Wang, W.T. Liou, D.J. Liaw, S.T. Huang, High glass transition and thermal stability of new pyridine-containing polyimides: effect of protonation on fluorescence, Polymer (Guildf). 49 (2008) 1538–1546, https://doi.org/10.1016/j.polymer.2008.01.039.
[14] M.H. Choi, K.W. Song, D.K. Moon, J.R. Haw, Effect of side chains on solubility and morphology of poly(benzodithiohene-alt-alkylbithiophene) in organic photovoltaics, J. Ind. Eng. Chem. 29 (2015) 120–128.
[15] M. Melucci, P. Frère, M. Allain, E. Levillain, G. Barbarella, J. Roncali, Molecular engineering of hybrid π-conjugated oligomers combining 3,4-ethylenedioxythiophene (EDOT) and thiophene-S,S-dioxide units, Tetrahedron 63 (2007) 9774–9783, https://doi.org/10.1016/j.tet.2007.07.006.
[16] S.-H. Wu, J.-H. Chen, C.-H. Shen, C.-C. Hsu, R.C.-C. Tsiang, Conjugated and partially conjugated 2,5-diphenylthiophene-containing light-emitting copolymers in polymeric light-emitting diode (PLED) device fabrications, J. Polym. Sci. Part A Chem. 42 (2004) 6061–6070, https://doi.org/10.1002/pola.20444.
[17] S. Iqbal, S. Ahmad, Recent development in hybrid conducting polymers: synthesis, applications and future prospects, J. Ind. Eng. Chem. 60 (2018) 53–84, https://doi.org/10.1016/j.jiec.2017.09.038.
[18] S.H. Yoon, J. Shin, H.A. Um, T.W. Lee, M.J. Cho, Y.J. Kim, Y.H. Son, J.H. Yang, G. Chae, J.H. Kwon, D.H. Choi, Novel 9,9"-(1,3-phenylene)bis-9H-carbazole-containing copolymers as hole-transporting and host materials for blue phosphorescent polymer light-emitting diodes, J. Polym. Sci. Part A Polym. Chem. 52 (2014) 707–718, https://doi.org/10.1002/pola.27054.
[19] D. Braun, G. Gustafsson, D. McBranch, A.J. Heeger, Electroluminescence and electrical transport in poly(3-octylthiophene) diodes, J. Appl. Phys. 72 (1992) 564–568, https://doi.org/10.1063/1.351834.
[20] J. b Sun, J. b Yang, C. Zhang, H. b Wang, J. b Li, S. Su, H. b Xu, T. b Zhang, Y. b Wu, W.Y. Wong, Bb. Xu, A novel white-light-emitting conjugated polymer derived from polyfluorene with a hyperbranched structure, New J. Chem. 39 (2015) 5180–5188, https://doi.org/10.1039/c5nj00289c.
[21] S.-H. Jin, H.-H. Jung, C.-K. Hwang, D.-S. Koo, W.S. Shin, Y.-I. Kim, J.W. Lee, Y.-S. Gal, High electroluminescent properties of conjugated copolymers from poly[9,9-dioctylfluorenyl-2,7-vinylene]-co-(2-(3-dimethyldodecylsilylphenyl)-1,4-phenylene vinylene)] for light-emitting diode applications, J. Polym. Sci. Part A Polym. Chem. 43 (2005) 5062–5071, https://doi.org/10.1002/pola.20994.
[22] J.Y. Lee, M.H. Choi, D.K. Moon, J.R. Haw, Synthesis of fluorene- and anthracene-based π-conjugated polymers and dependence of emission range and luminous efficiency on molecular weight, J. Ind. Eng. Chem. 16 (2010) 395–400, https://doi.org/10.1016/j.jiec.2009.08.003.
[23] N. Pilicode, N.K. m, S.M. n, A.V. Adhikari, New cyanopyridine based conjugative polymers as blue emitters: synthesis, photophysical, theoretical and electroluminescence studies, J. Photochem. Photobiol. A 364 (2018) 6–15, https://doi.org/10.1016/j.jphotochem.2018.05.037.
[24] B. Hemavathi, T.N. Ahipa, S. Pillai, R.K. Pai, Cyanopyridine based conjugated polymer-synthesis and characterization, Polymer 78 (2015) 22–30, https://doi.org/10.1016/j.polymer.2015.09.053.
[25] M.G. Murali, P. Naveen, D. Udayakumar, V. Yadav, R. Srivastava, Synthesis and characterization of thiophene and fluorene based donor-acceptor conjugated polymer containing 1,3,4-oxadiazole units for light-emitting diodes, Tetrahedron Lett. 53 (2012) 157–161, https://doi.org/10.1016/j.tetlet.2011.10.157.
[26] N. Martin, J.L. Segura, C. Seoane, E. Orti, P.M. Viruela, R. Viruela, A. Albert, F.H. Cano, J. VidalGancedo, C. Rovira, J. Veciana, Synthesis, characterization, and theoretical study of sulfur- containing donor-acceptor DCNQI derivatives with photoinduced intramolecular electron transfer, J. Org. Chem. 61 (1996) 3041–3054.
[27] D. Bondarev, J. Zedník, Influence of covalent structure and molecular weight distribution on the optical properties of alternating copolymers and oligomers with 1,2,3-triazole and 1,3,4-oxadiazole side groups, Polymer 124 (2017) 107–116, https://doi.org/10.1016/j.polymer.2017.07.045.
[28] A.D. Becke, A new mixing of Hartree-Fock and local density-functional theories, J. Chem. Phys. 98 (1993) 1372–1377, https://doi.org/10.1063/1.464304.
[29] P. Naik, M.R. Elmorsy, R. Su, D.D. Babu, A. El-Shafei, A.V. Adhikari, New carbazole based metal-free organic dyes with D-π-A-π-A architecture for DSSCs: synthesis, theoretical and cell performance studies, Sol. Energy 153 (2017) 600–610, https://doi.org/10.1016/j.solener.2017.05.088.
[30] P. Naik, R. Su, M.R. Elmorsy, A. El-Shafei, A.V. Adhikari, New carbazole based dyes as effective co-sensitizers for DSSCs sensitized with ruthenium (II) complex (NCSU-10), J. Energy Chem. 27 (2018) 351–360, https://doi.org/10.1016/j.jechem.2017.12.013.
[31] P. Naik, R. Su, M.R. Elmorsy, A. El-Shafei, A.V. Adhikari, Investigation of new carbazole based metal-free dyes as active photo-sensitizers/co-sensitizers for DSSCs, Dye Pigm. 149 (2018) 177–187, https://doi.org/10.1016/j.dyepig.2017.09.068.
[32] M.G. Murali, A.D. Rao, P.C. Ramamurthy, New low band gap 2-(4-(trifluoromethyl) phenyl)-1H-benzo[d]imidazole and benzo[1,2-c;4,5-c′]bis[1,2,5]thiadiazole based conjugated polymers for organic photovoltaics, RSC Adv. 4 (2014) 44902–44910, https://doi.org/10.1039/C4RA08214A.
[33] J.H. Burroughes, D.D.C. Bradley, A.R. Brown, R.N. Marks, K. Mackay, R.H. Friend, P.L. Burns, A.B. Holmes, Light-emitting diodes based on conjugated polymers, Nature 347 (1990) 539–541, https://doi.org/10.1038/347539a0.
[34] B.M.T. Bernius, M. Inbasekaran, J.O. Brien, W. Wu, Progress with light-emitting polymers, Adv. Mater. (2000) 1737–1750, https://doi.org/10.1002/1521-4095(200012)12:23<1737::AID-ADMA1737>3.0.CO;2-N.
[35] R.H. Friend, R.W. Gymer, A.B. Holmes, J.H. Burroughes, R.N. Marks, C. Taliani, D.D.C. Bradley, D.A.D. Santos, J.L. Brédas, M. Lögdlund, W.R. Salaneck, Electroluminescence in conjugated polymers, Nature 397 (1999) 121–128, https://doi.org/10.1038/16393.
[36] F. Chen, P.G. Mehta, L. Takiff, R.D. McCullough, Improved electroluminescence performance of poly (3-alkylthiophenes) having a high head-to-tail (HT) ratio, J. Mater. Chem. 6 (1996) 1763–1766, https://doi.org/10.1039/JM9960601763.
[37] H.J. Jiang, J.L. Zhang, J. Sun, W. Huang, Novel amphipathic photoluminescent copolymers containing fluorene, pyridine and thiophene moieties: synthesis, characterization and self-assembly, Polymer 53 (2012) 5684–5690, https://doi.org/10.1016/j.polymer.2012.10.007.
[38] J. He, L. Du, C. Wang, M. Jiang, L. Liu, Y. Mo, Z. Xie, B. Yang, Y. Ma, Conformation pre-organization in fluorene-based conjugated polymer for simultaneous enhancement of luminescence and charge mobility, Polym. Chem. 8 (2017) 1255–1262, https://doi.org/10.1039/c6py01995a.
[39] J.H. Cook, J. Santos, H. Li, H.A. Al-Attar, M.R. Bryce, A.P. Monkman, Efficient deep blue fluorescent polymer light-emitting diodes (PLEDs), J. Mater. Chem. C 2 (2014) 5587–5592, https://doi.org/10.1039/c4tc00896k.
[40] B. Liu, S. Ye, Y. Zou, B. Peng, Y. He, K. Zhou, A dithienyl benzotriazole-based polyfluorene: synthesis and applications in polymer solar cells and red light-emitting diodes, Macromol. Chem. Phys. 212 (2011) 1489–1496, https://doi.org/10.

1002/macp.201100080.
[41] J.H. Park, N.S. Cho, Y.K. Jung, H.J. Cho, H.K. Shim, H. Kim, Y.S. Lee, Polymeric light emitting properties and structural relationships of fluorene-based conjugated copolymers containing various hole transporting derivatives, Org. Electron. Phys. Mater. Appl. 8 (2007) 272–285, https://doi.org/10.1016/j.orgel.2006.08.002.
[42] R.H. Lee, L.W. Liu, Electroluminescence and photovoltaic properties of light-emitting devices and solar cells comprising 2-pyran-4-ylidene-malononitrile conjugated polymers, Dyes Pigm. 84 (2010) 190–202, https://doi.org/10.1016/j.dyepig.2009.08.002.